

ARTICLE

Angulin-1 seals tricellular contacts independently of tricellulin and claudins

Taichi Sugawara^{1,2,3}, Kyoko Furuse¹, Tetsuhisa Otani^{1,2}, Tomohiko Wakayama³, and Mikio Furuse^{1,2}

Tricellular tight junctions (tTJs) are specialized tight junctions (TJs) that seal the intercellular space at tricellular contacts (TCs), where the vertices of three epithelial cells meet. Tricellulin and angulin family membrane proteins are known constituents of tTJs, but the molecular mechanism of tTJ formation remains elusive. Here, we investigated the roles of angulin-1 and tricellulin in tTJ formation in MDCK II cells by genome editing. Angulin-1-deficient cells lost the plasma membrane contact at TCs with impaired epithelial barrier function. The C terminus of angulin-1 bound to the TJ scaffold protein ZO-1, and disruption of their interaction influenced the localization of claudins at TCs, but not the tricellular sealing. Strikingly, the plasma membrane contact at TCs was formed in tricellulin- or claudin-deficient cells. These findings demonstrate that angulin-1 is responsible for the plasma membrane seal at TCs independently of tricellulin and claudins.

Introduction

Epithelia work as barriers to separate the internal body from the external environment and to generate distinct fluid compartments within the body for various organ functions. Tight junctions (TJs) restrict leakage of solutes through the paracellular pathway, contributing to the epithelial barrier function (Tsukita et al., 2001; Van Itallie and Anderson, 2014; Zihni et al., 2016). On ultrathin section EM, TJs appear as a series of apparent fusions between adjacent cell membranes that obliterate the intercellular space at the most apical part of the lateral membrane (Farquhar and Palade, 1963). On freeze-fracture EM, TJs are visualized as anastomosing intramembranous particle strands (TJ strands; Staehelin, 1973). Claudin family membrane proteins play key roles in TJ formation. Claudins assemble in cell–cell contacts between adjacent cells and polymerize within the plasma membrane to form TJ strands (Furuse et al., 1999; Sasaki et al., 2003). On the cytoplasmic side of TJs, the claudin C-termini directly bind to three TJ-scaffolding proteins: ZO-1, ZO-2, and ZO-3 (Itoh et al., 1999). These three proteins have domain structures that include three PDZ domains (PDZ1–3) for protein–protein interactions (Willott et al., 1993; Itoh et al., 1993). ZO-1 directly binds to claudins and junctional adhesion molecule-A (JAM-A) via its PDZ1 and PDZ3 domains, respectively (Itoh et al., 1999; Itoh et al., 2001), and to ZO-2 via its PDZ2 domain (Fanning et al., 1998). Importantly, ZO-1 and ZO-2 are required for claudin-based TJ formation in cultured epithelial cells (Umeda et al., 2006; Phua et al., 2014; Otani et al., 2019).

As well as the paracellular barrier formed by TJs between adjacent cells, epithelial cells need to obliterate the extracellular space at tricellular contacts (TCs), where the vertices of three cells meet, to establish full epithelial barrier function. TCs contain specialized TJs designated tricellular TJs (tTJs; Staehelin et al., 1969; Staehelin, 1973; Wade and Karnovsky, 1974; Walker et al., 1985; Ikenouchi et al., 2005). In freeze-fracture replicas, the most apical elements of TJ strands in bicellular TJs join together at TCs, turn, and extend in the basal direction attached to one another (Staehelin, 1973). Each vertical TJ strand along the apicobasal axis is called a “central sealing element.” Three central sealing elements at a TC squeeze the extracellular space to form a central tube of ~10-nm diameter, considered to work as a diffusion barrier (Staehelin, 1973). Short TJ strands are often connected to the central sealing elements in freeze-fracture replicas (Staehelin, 1973). Tricellulin and angulin family proteins, including angulin-1/lipolysis-stimulated lipoprotein receptor (LSR), angulin-2/ILDR1, and angulin-3/ILDR2, have been identified as molecular constituents of tTJs (Ikenouchi et al., 2005; Masuda et al., 2011; Higashi et al., 2013). Tricellulin is a four-transmembrane protein with structural similarity to occludin (Ikenouchi et al., 2005), while angulins are type I transmembrane proteins with a single Ig-like domain (Masuda et al., 2011; Higashi et al., 2013). Tricellulin and angulins localize along the central sealing elements of tTJs (Ikenouchi et al., 2005;

¹Division of Cell Structure, National Institute for Physiological Sciences, National Institute of Natural Sciences, Okazaki, Aichi, Japan; ²Department of Physiological Sciences, The Graduate University for Advanced Studies, SOKENDAI, Okazaki, Aichi, Japan; ³Department of Histology, Graduate School of Medical Sciences, Kumamoto University, Kumamoto, Japan.

Correspondence to Mikio Furuse: furuse@nips.ac.jp.

© 2021 Sugawara et al. This article is distributed under the terms of an Attribution–Noncommercial–Share Alike–No Mirror Sites license for the first six months after the publication date (see <http://www.rupress.org/terms/>). After six months it is available under a Creative Commons License (Attribution–Noncommercial–Share Alike 4.0 International license, as described at <https://creativecommons.org/licenses/by-nc-sa/4.0/>).

Masuda et al., 2011). Because angulins recruit tricellulin to TCs (Masuda et al., 2011; Higashi et al., 2013), the angulin–tricellulin axis is proposed to play crucial roles in tTJ formation (Furuse et al., 2014). RNAi-mediated suppression of tricellulin or angulin-1 expression in EpH4 mouse mammary epithelial cells was shown to impair epithelial barrier function (Ikenouchi et al., 2005; Masuda et al., 2011). In vivo studies revealed that tricellulin or angulin-2 gene mutations cause human nonsyndromic hearing loss (DFNB49 or DFNB42, respectively; Riazuddin et al., 2006; Borck et al., 2011), while tricellulin- or angulin-2-deficient mice show progressive hearing loss associated with hair cell degeneration (Kamitani et al., 2015; Higashi et al., 2015; Morozko et al., 2015; Sang et al., 2015). Angulin-2-deficient mice were reported to suffer from polyuria and polydipsia arising from renal concentrating defects (Gong et al., 2017), while this phenotype was not observed in another study (Hempstock et al., 2020). Meanwhile, angulin-1-deficient mouse embryos die before embryonic day 15.5 (Mesli et al., 2004) and exhibit blood–brain barrier leakage (Sohet et al., 2015).

Despite accumulating evidence on the physiological roles of tTJ-associated proteins, the molecular mechanism for tTJ formation remains to be solved. It is currently unclear whether the central sealing elements in tTJs contain TJ components such as claudins, occludin, and ZO-1 because of the lack of detailed immunolocalization analyses. Furthermore, the molecules responsible for obliteration of the paracellular gap at TCs have not been clarified. To address these issues, it is useful to analyze the ultrastructure of tTJs in tricellulin- or angulin-deficient cultured epithelial cells such as MDCK cells, which have contributed to investigations on structure–function relationships in TJs (Cerejido et al., 1978; Stevenson et al., 1988; Sonoda et al., 1999).

In this study, we examined the roles of angulin-1 and tricellulin in tTJ formation and epithelial barrier function by generating angulin-1- and tricellulin-deficient MDCK II cells using genome editing. We demonstrate that angulin-1 is required for the plasma membrane contact at TCs and recruits claudins to TCs through its interaction with ZO-1. We further show that the plasma membrane contact at TCs occurs independently of claudin-based TJ strands. Finally, we demonstrate that tricellulin is not essential for the plasma membrane contact at TCs or epithelial barrier function. Taken together, we conclude that angulin-1 plays pivotal roles in the plasma membrane seal at TCs for tTJ formation independently of tricellulin and claudins.

Results

Visualization of apicobasal extension of tTJs by fluorescence microscopy

To examine the detailed distributions of tTJ and TJ proteins at TCs, we performed immunofluorescence staining of frozen mouse kidney and small intestine sections using antibodies against tTJ and TJ proteins. In renal tubules in the kidney, TJs and tTJs locate at the luminal side of narrow epithelial tubes. Upon close inspection of collecting duct epithelial cells, tricellulin was detected as rodlike signals extending from the intersection of TJ markers, including claudin-8, occludin, and ZO-1 (i.e., TC),

and appeared to merge with one of the branches of TJ markers extending in the basal direction (Fig. 1 A). Angulin-2 was colocalized with tricellulin (Fig. 1). Meanwhile, tricellulin and angulin-1 were detected as dots at TCs in claudin-2–positive proximal tubule epithelial cells (Fig. S1, A and B). In the mouse small intestine, tricellulin and angulin-1 often extended from the tricellular intersections of claudin-15, occludin, or ZO-1 as rods, with which each TJ marker was colocalized (Fig. 1 B). Next, we examined the distributions of tTJ and TJ proteins in MDCK II cells cultured on Transwell filters. In the image acquisition by confocal laser microscopy, we focused on confocal sections at two regions: the apical region, in which TJ markers were highly concentrated, and the lateral region, which was more basal than the apical region and did not contain TJ markers. The relationship between the structural organization of tTJs and the confocal sections is shown in Fig. 2 A. By immunofluorescence, tricellulin and angulin-1 were clearly detected at TCs in MDCK II cells, with relatively weak staining in the apical region and more intense staining in the lateral region. Also, weak signals of angulin-1 were observed in the lateral membrane (Fig. 2, B–E). In Z-stack confocal images, tricellulin and angulin-1 showed extended distributions along the apicobasal axis at TCs (Fig. 2 F). Furthermore, claudin-2, occludin, and ZO-1 were colocalized with tTJ markers along the apicobasal axis at TCs (Fig. 2, B–E). ZO-2 and ZO-3 also showed extended localization with ZO-1 at TCs (Fig. S1, C and D). JAM-A was localized not only at apical junctions but also at the lateral plasma membrane domain in MDCK II cells, and its specific concentration along the apicobasal axis at TCs was not clearly detected (Fig. S1 E). Taken together, these observations indicate that TJ proteins are incorporated into tTJs, the outlines of which can be visualized by light microscopy using tTJ markers.

Apicobasal extension of adherens junction (AJ) components at TCs

AJs occur just beneath TJs at bicellular contacts in vertebrates (Farquhar and Palade, 1963), but their distribution at TCs has not been described yet. Therefore, we examined the localization of AJ components, including E-cadherin, α -catenin, and afadin, at TCs in MDCK II cells by immunofluorescence staining. E-cadherin and α -catenin were distributed at the cell boundary not only at the apical region but also at lateral regions in confocal sections, and they did not show remarkable concentration at TCs (Fig. 3, A and B). However, when α -catenin was labeled with the α -18 mAb, which recognizes a tension-dependent α -catenin epitope (Yonemura et al., 2010), its concentrated signal was detected not only along bicellular contacts in the apical region but also along the apicobasal axis at TCs colocalizing with claudin-2 (Fig. 3 C). Afadin also showed junctional localization at the apical region and rodlike extension along the apicobasal axis at TCs (Fig. 3 D). These results suggest that AJs are located with tTJs along the apicobasal axis at TCs.

Angulin-1 is essential for the plasma membrane contact at TCs and epithelial barrier function in MDCK II cells

To examine the role of angulins in tTJ formation, we generated angulin-deficient MDCK II cells. Expression of angulin-1 and

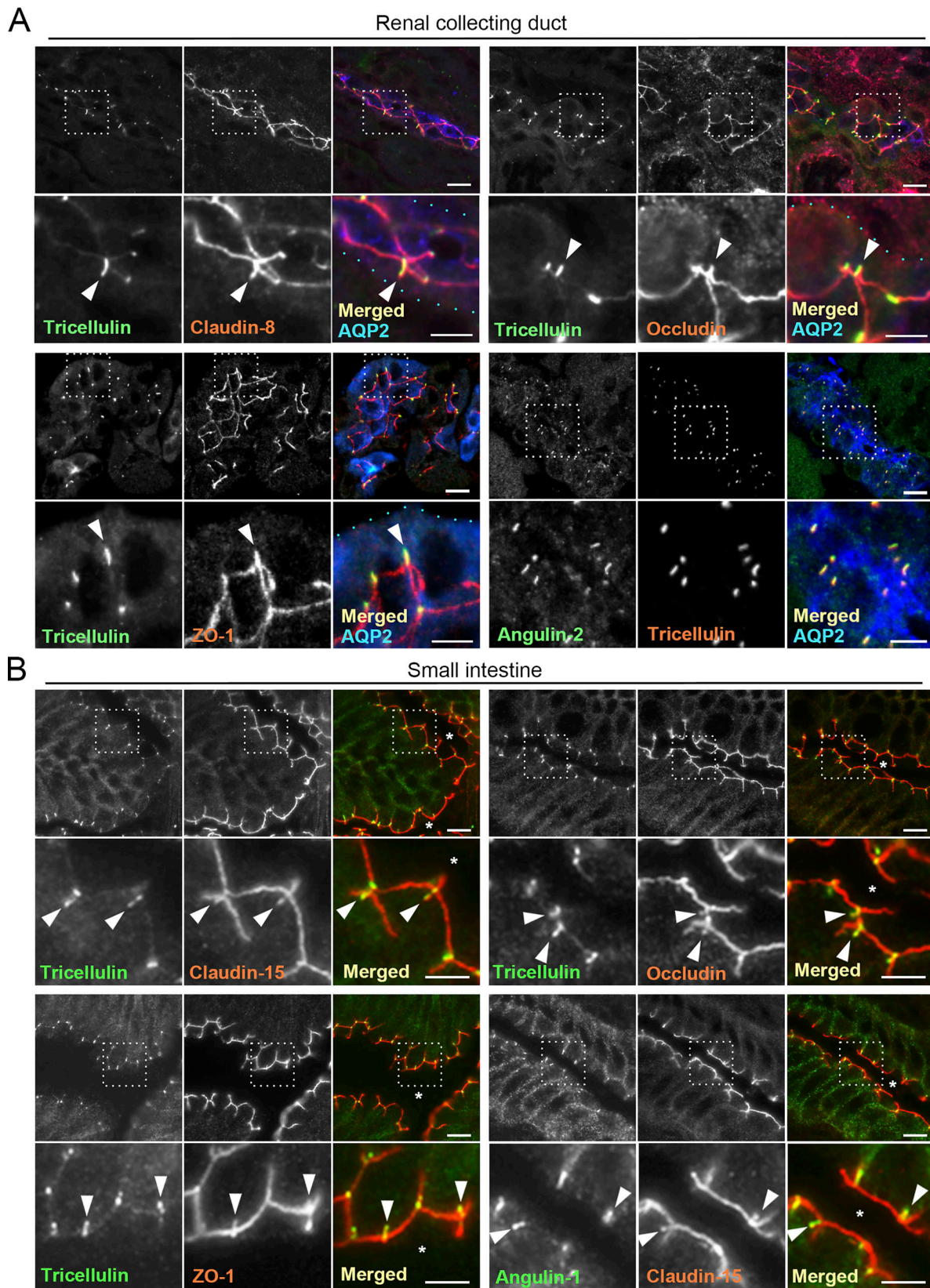


Figure 1. **Localization of tTJ and TJ proteins in the mouse kidney and small intestine.** (A) Triple-immunofluorescence staining of frozen mouse kidney sections containing collecting ducts with anti-tricellulin mAb, anti-claudin-8 pAb, and anti-AQP-2 pAb (top left); anti-tricellulin mAb, anti-occludin pAb, and anti-AQP-2 pAb (top right); anti-tricellulin mAb, anti-ZO-1 pAb, and anti-AQP-2 pAb (bottom left); and anti-angulin-2 pAb, anti-tricellulin mAb, and anti-AQP-2 pAb (bottom right). AQP-2 staining is only shown in the merged images. The boxed regions are magnified on the bottom. Tricellulin shows rodlike staining in AQP-2-positive collecting ducts. Claudin-8, occludin, and ZO-1 colocalize with tricellulin at TCs (arrowheads). Light blue dots in the magnified merged images

indicate the outline of collecting ducts. **(B)** Double-immunofluorescence staining of frozen mouse small intestine sections with anti-tricellulin mAb and anti-claudin-15 pAb (top left), anti-tricellulin mAb and anti-occludin pAb (top right), anti-tricellulin mAb and anti-ZO-1 pAb (bottom left), and anti-angulin-1 mAb and anti-claudin-15 pAb (bottom right). Asterisks show the intestinal lumen. The boxed regions are magnified on the bottom. Bars: 10 μ m (top), 5 μ m (bottom).

angulin-2 was previously demonstrated in MDCK cells by RNA-sequencing analysis, with much higher expression of angulin-1 than of angulin-2 (Shukla et al., 2015). Thus, we focused on angulin-1 in the present study. We disrupted the angulin-1-encoding gene in MDCK II cells by TALEN (transcription activator-like effector nuclease)-mediated genome editing and established two independent angulin-1-knockout (KO) cell clones: angulin-1-KO_1 and angulin-1-KO_2 (Fig. 4 A and Fig. S2 A). Because the two clones had essentially the same phenotype, we present data for angulin-1-KO_1 cells as representatives of angulin-1-KO cells unless otherwise specified. Immunofluorescence staining revealed that TC localization of tricellulin was impaired in angulin-1-KO cells (Fig. 4 B), supporting the idea that angulin-1 is the major angulin subtype in MDCK II cells. In angulin-1-KO cells, concentrated localization of claudin-2 and ZO-1 were detected in the apical region containing TJs, but not in the lateral region at TCs (Fig. 4 C). Reexpression of angulin-1 in angulin-1-KO cells restored the extended distributions of claudin-2 and ZO-1 along the apicobasal axis at TCs in Z-stack confocal images (Fig. 4, C and D; and Fig. S2 B). These results suggest that angulin-1 is required for vertically extended localization of TJ proteins at TCs.

Next, we examined the epithelial barrier function in angulin-1-KO cells cultured on Transwell filters. Paracellular flux of fluorescein (332 D) was increased in angulin-1-KO cells compared with MDCK II cells (Fig. 4 E), and the increase was abolished by reexpression of mouse angulin-1 (Fig. 4 F). Meanwhile, transepithelial electrical resistance (TER), reflecting electrolyte permeability, was not significantly altered in angulin-1-KO cells (Fig. S2 C). The low TER in MDCK II cells arising from endogenous claudin-2, which forms cation-selective pores in TJs (Furuse et al., 2001; Amasheh et al., 2002; Tokuda and Furuse, 2015), may hamper detection of subtle differences in TER measurements. This prompted us to further examine the impact of angulin-1 on electrolyte permeability. We disrupted the angulin-1 gene by CRISPR/Cas9-mediated genome editing in claudin-2-deficient MDCK II cells (claudin-2-KO cells) with high TER (Tokuda and Furuse, 2015) and established three angulin-1/claudin-2-double-KO (dKO) cell clones (Fig. S3, A and B). In all three clones, TER was remarkably decreased, and paracellular flux of fluorescein was increased, compared with control claudin-2-KO cells (Fig. S3, C and D). In these cells, we could not observe any reduction of claudin-4, a barrier-forming claudin (Fig. S3 E). Reexpression of angulin-1 in angulin-1/claudin-2-dKO cells restored the TER and flux of fluorescein to the levels in claudin-2-KO cells (Fig. S3, F-H). These findings suggest that angulin-1 plays crucial roles in epithelial barrier formation in MDCK II cells.

To investigate whether the reduction of the epithelial barrier function in angulin-1-deficient cells is caused by disorganization of tTJ ultrastructure, we prepared horizontal ultrathin sections

of cells cultured on Transwell filters for transmission EM. Intriguingly, the extracellular space at TCs was almost completely closed by the contact between the three plasma membranes in MDCK II cells. This occurred at not only the level containing TJs (TJ level) but also a more basal level where desmosomes, but not TJs, were observed (desmosome level; Fig. 5 A). The structures appeared to correspond to the tTJs previously described by freeze-fracture EM (Staehelin, 1973). In contrast, no plasma membrane contact was observed at TCs in angulin-1-KO cells. Instead, an apparent gap was observed at TCs in both the TJ and desmosome levels (Fig. 5 A). Reexpression of angulin-1 in angulin-1-KO cells restored the plasma membrane contact at TCs (Fig. 5 A). Similar gaps at TCs were also observed in horizontal ultrathin sections of angulin-1/claudin-2-dKO cells (Fig. S3 I). We further examined the tTJ ultrastructure by freeze-fracture EM. In MDCK II cells, typical tTJs with the central sealing elements and short TJ strands connected to these elements were observed (Fig. 5, B₁, B₁', and B₂). The depth of the tTJs varied. In contrast, TCs in angulin-1-KO cells had two vertical TJ strands separated from one another by smooth fracture planes of the plasma membranes (Fig. 5, B₃, B₃', and B₄). TJ strands along bicellular contacts were continuous in angulin-1-KO cells (Fig. 5 B₅). These results demonstrate that angulin-1 is required for the plasma membrane contact at TCs and the central sealing elements of tTJs.

PDZ domain-binding motif (pbm) of angulin-1 is required for extended localization of TJ constituents at TCs via ZO-1 binding

Angulin family proteins have a putative pbm at their C-terminus (Higashi et al., 2013). However, it is unknown which molecules the pbm interacts with and how the putative interactions contribute to tTJ formation. To examine the role of the angulin-1 pbm, we established angulin-1-KO cells stably expressing an angulin-1 mutant lacking the C-terminus five amino acids (angulin-1 Δ pbm; Fig. 6 A and Fig. S2 B). On immunofluorescence staining, angulin-1 Δ pbm was localized at TCs and extended along the apicobasal axis with tricellulin (Fig. 6 B). Meanwhile, ZO-1 and claudin-2 were localized at the TJ level only and did not colocalize with angulin-1 Δ pbm along the apicobasal axis at TCs (Fig. 6, B and C). These results suggest that the angulin-1 pbm is responsible for the extended distribution of TJ constituents at TCs.

Next, we examined the roles of angulin-1 pbm in the epithelial barrier function and plasma membrane contact formation at TCs. As shown in Fig. 6 D, the expression of angulin-1 Δ pbm in angulin-1-KO cells reduced paracellular flux of fluorescein. Consistently, introduction of angulin-1 Δ pbm to angulin-1/claudin-2-dKO cells increased TER and suppressed paracellular flux of fluorescein (Fig. S3, F-H). In horizontal ultrathin sections of angulin-1 Δ pbm-expressing angulin-1-KO cells, the extracellular

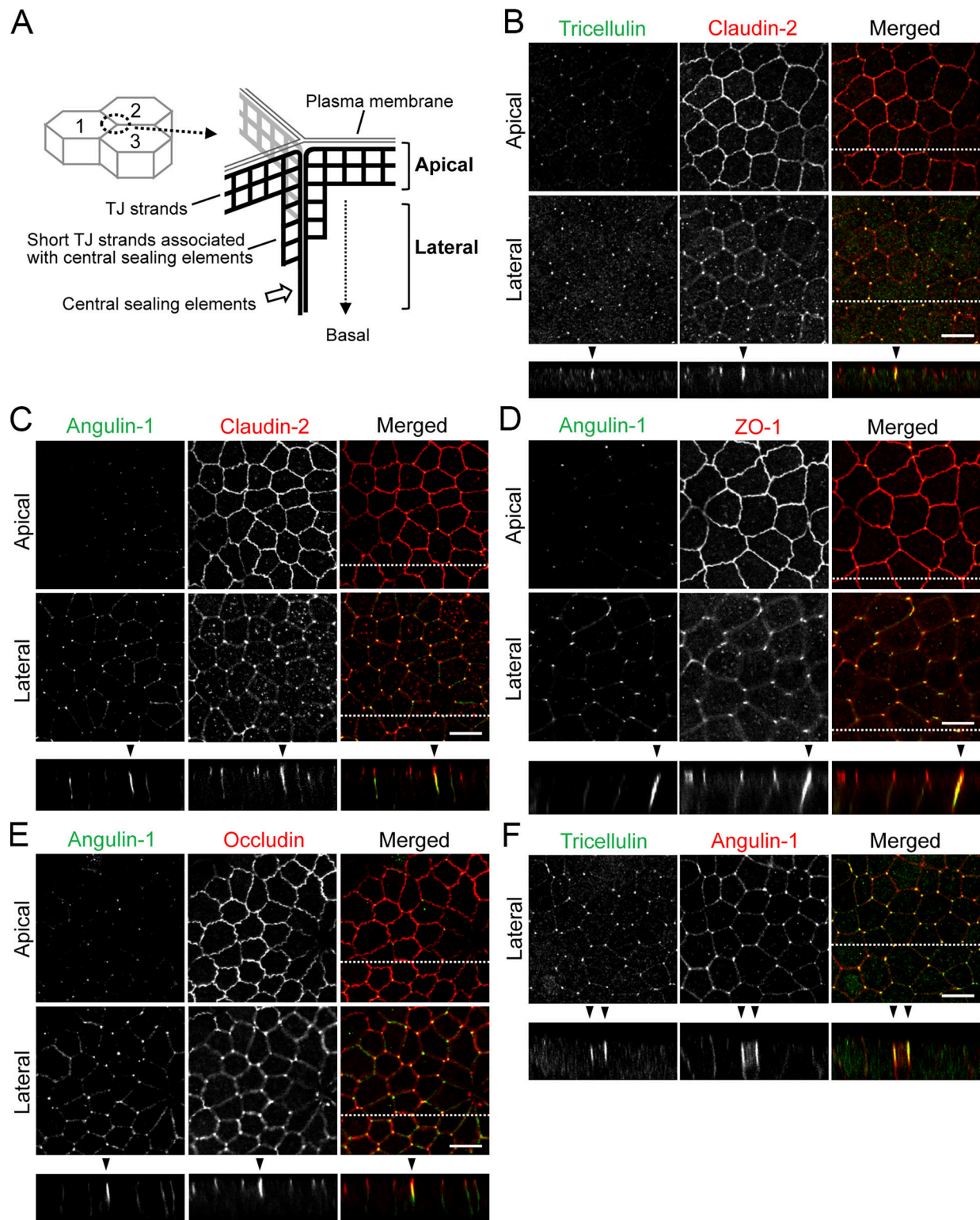


Figure 2. **Localization of tTJ and TJ proteins at TCs in MDCK II cells.** (A) Supposed relationship between tTJ structural organization and confocal sections in the apical and lateral regions. The scheme represents tTJs observed from the inside of cell 3. The network of black bold lines represents TJ strands. The most apical elements of TJ strands in bicellular TJs join together at TCs, turn, and extend in the basal direction attached to one another to form the central sealing elements that connect with short TJ strands. The confocal sections in the apical region correspond to the level of bicellular TJs, while those in the lateral region are more basal and do not contain bicellular TJs. (B–F) Double-immunofluorescence staining of MDCK II cells with anti-tricellulin pAb and anti-claudin-2 mAb (B), anti-angulin-1 pAb and anti-claudin-2 mAb (C), anti-angulin-1 pAb and anti-ZO-1 mAb (D), anti-angulin-1 pAb and anti-occludin mAb (E), and anti-tricellulin mAb and anti-angulin-1 pAb (F). Confocal sections in the apical region, including TJ markers and the lateral region, together with the corresponding Z-stack images along the white dotted lines are shown. Not only tricellulin and angulin-1 but also claudin-2, occludin, and ZO-1 show extended localization along the apicobasal axis at TCs (arrowheads). Bar: 10 μ m.

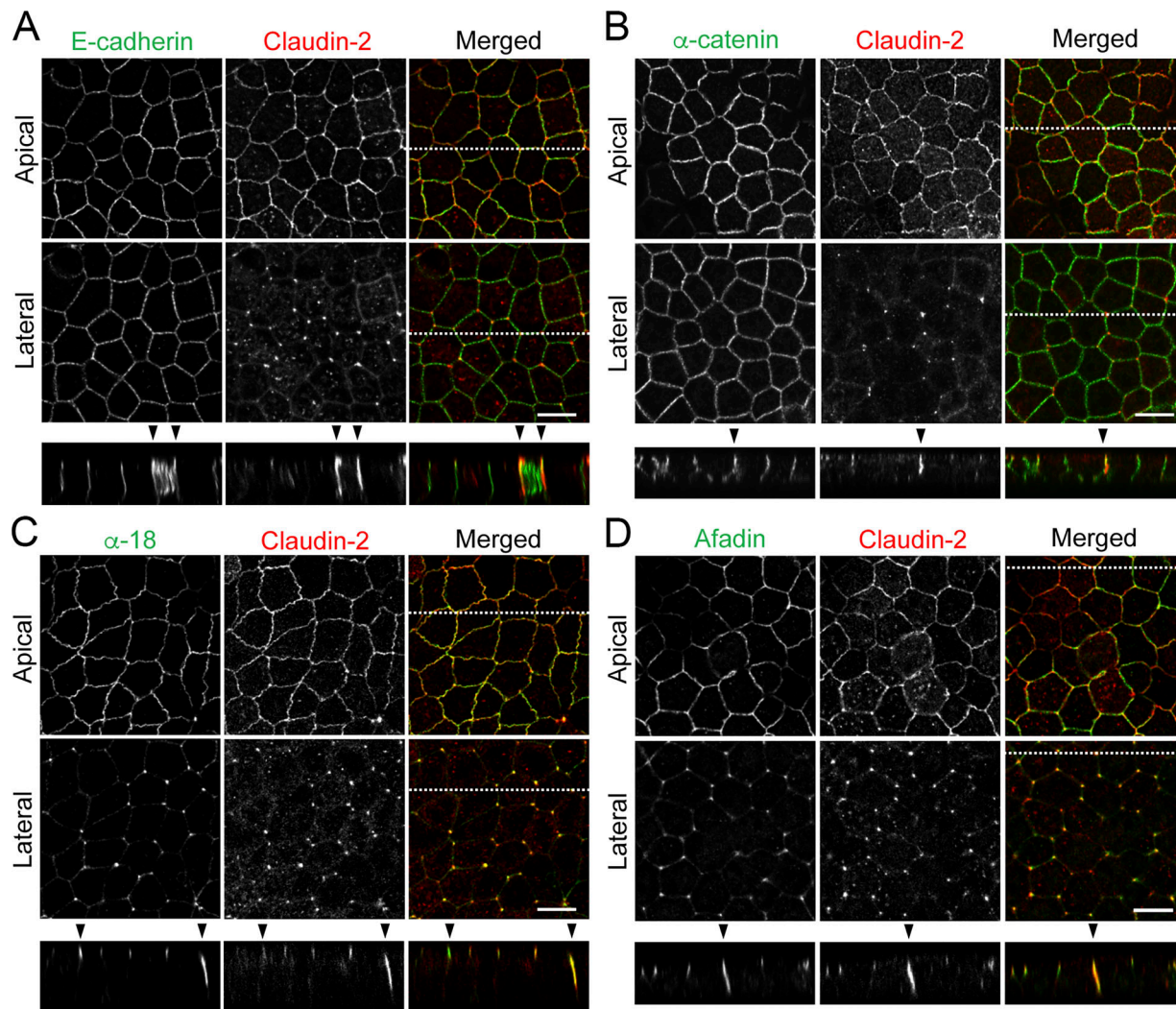


Figure 3. Localization of TJ and AJ proteins at TCs in MDCK II cells. (A–D) Double-immunofluorescence staining of MDCK II cells with anti-claudin-2 mAb and anti-E-cadherin mAb (A), anti- α -catenin pAb (B), anti-tension-dependent epitope of α -catenin mAb (α -18; C), and anti-afadin pAb (D). Confocal sections in the apical region, including claudin-2 signals at bicellular contacts and the lateral region, together with the corresponding Z-stack images along the white dotted lines are shown. α -18 under tension and afadin show extended localization along the apicobasal axis at TCs (arrowheads). Bar: 10 μ m.

space in TCs at not only the TJ level but also the desmosome level was sealed by the plasma membranes (Fig. 6 E). These results suggest that the angulin-1 pbm is not essential for the epithelial barrier function or plasma membrane contact at TCs.

To further investigate the mechanism of apicobasal extension of claudin-2 and ZO-1 via the angulin-1 pbm, we hypothesized that the angulin-1 pbm binds to the PDZ domains of ZO proteins. We generated bacterial GST fusion proteins of the C-terminus 167 amino acids (aa 409–575) of mouse angulin-1 and its deletion mutant lacking the C-terminus 5 amino acids corresponding to the pbm (aa 409–570), designated GST-ang575 and GST-ang570, respectively. Pull-down assays revealed that GST-ang575, but not GST-ang570, interacted with ZO-1, ZO-2, and ZO-3 in angulin-1-KO cell lysates (Fig. 7 A), suggesting that the angulin-1 pbm binds to ZO family proteins. We also attempted coimmunoprecipitation experiments from MDCK II cells but were unsuccessful, possibly due to the poor solubility of TJ components (data not shown). Thus, we focused on ZO-1 as a possible

binding partner of angulin-1. We performed pull-down assays with GST-ang575 and a bacterial maltose-binding protein (MBP) fusion protein of aa 1–862 of mouse ZO-1 containing three PDZ domains (MBP-N-ZO-1; Fig. 7 B). We found that GST-ang575, but not GST, bound to MBP-N-ZO-1 (Fig. 7 C). To determine which PDZ domain of ZO-1 binds to angulin-1, we generated bacterial MBP fusion proteins of aa 19–113, aa 181–292, and aa 423–503 of mouse ZO-1, corresponding to PDZ1, PDZ2, and PDZ3, respectively (Fig. 7 B). In pull-down assays, GST-ang575 bound to the MBP fusion protein of PDZ2, but not to those of PDZ1 or PDZ3 (Fig. 7 D), suggesting that angulin-1 directly binds to PDZ2 of ZO-1 via its pbm.

Next, we examined the role of the interaction between the angulin-1 pbm and PDZ2 of ZO-1. In ZO-1/ZO-2-dKO MDCK II cells, which lack not only TJs but also beltlike AJs (Otani et al., 2019), angulin-1 was not localized at TCs (Fig. S4 A). However, when GFP-tagged full-length ZO-1 (ZO-1-GFP) or its mutant lacking the PDZ2 domain (ZO-1 Δ PDZ2-GFP) was stably introduced

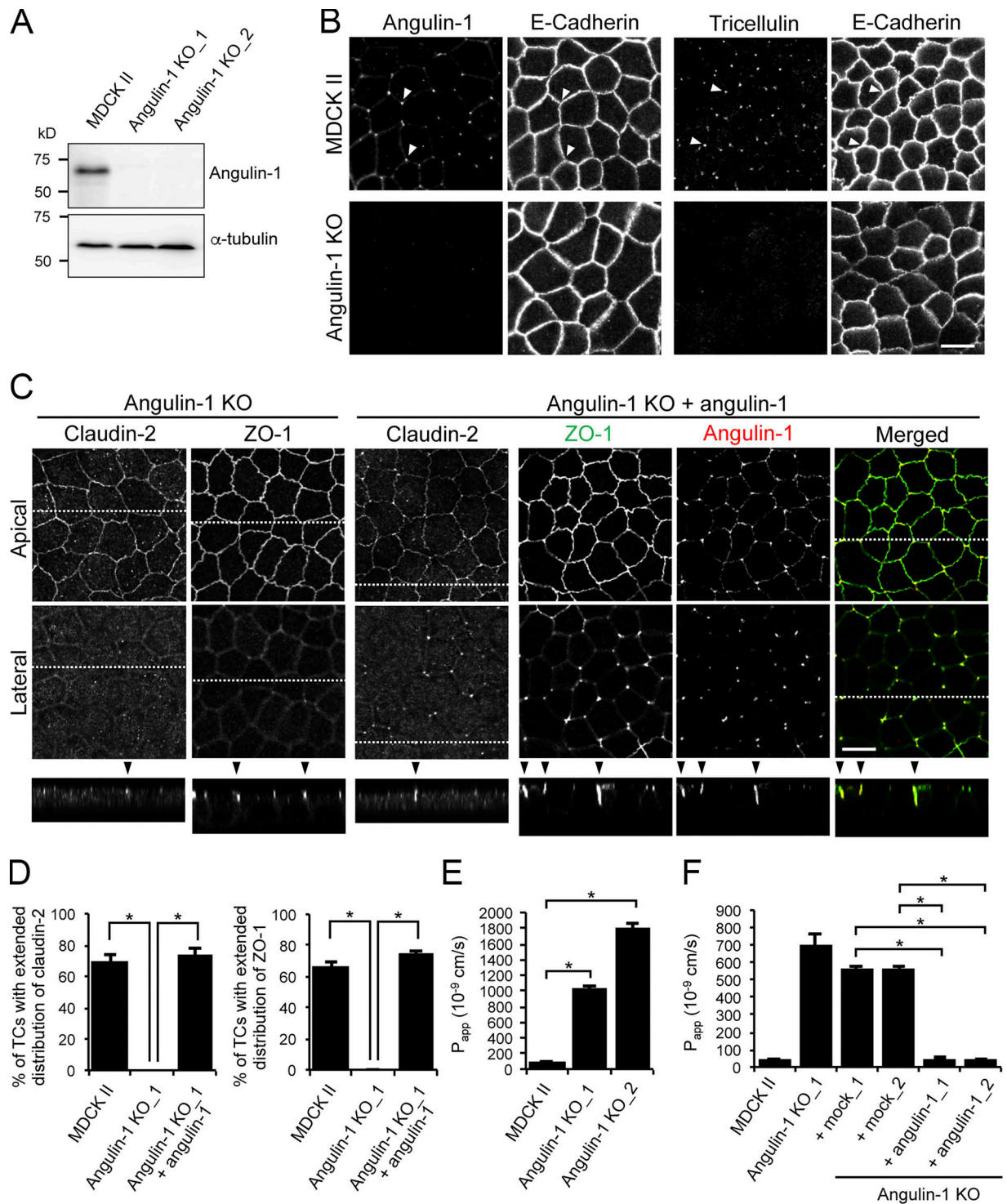


Figure 4. Role of angulin-1 in the localization of TJ proteins at TCs and epithelial barrier function. (A) Western blotting of lysates of MDCK II cells and two independent angulin-1-KO cell clones (angulin-1-KO_1 and -KO_2) with anti-angulin-1 pAb or anti- α -tubulin mAb. (B) Double-immunofluorescence staining of MDCK II cells and angulin-1-KO cells with anti-angulin-1 pAb and anti-E-cadherin mAb or anti-tricellulin pAb and anti-E-cadherin mAb. Arrowheads indicate TCs. (C) Immunofluorescence staining of angulin-1-KO cells and angulin-1-KO cells expressing exogenous angulin-1 (angulin-1-KO + angulin-1). Angulin-1-KO cells were immunostained with anti-claudin-2 mAb or anti-ZO-1 mAb. Angulin-1-KO cells expressing exogenous angulin-1 were singly immunostained with anti-claudin-2 mAb or doubly stained with anti-ZO-1 mAb and anti-angulin-1 pAb. Confocal sections of the apical region, including TJ markers and the lateral region, together with the corresponding Z-stack images along the white dotted lines are shown. Arrowheads indicate TCs. (D) Quantification of TCs with extended distribution of fluorescence signals of claudin-2 and ZO-1 to the basal direction. (E) Paracellular flux of fluorescein in MDCK II cells and two independent angulin-1-KO cell clones (angulin-1-KO_1 and -KO_2). P_{app} , apparent permeability. (F) Paracellular flux of fluorescein in MDCK II cells, angulin-1-KO cells, two independent mock-transfected angulin-1-KO cell clones (+mock_1 and +mock_2), and two independent angulin-1-KO cell clones expressing exogenous angulin-1 (+angulin-1_1 and +angulin-1_2). Data are shown as mean \pm SD ($n = 3$) and were analyzed by Tukey-Kramer test (D and F) or Dunnett's test (E). *, $P < 0.01$. Bars: 10 μ m.

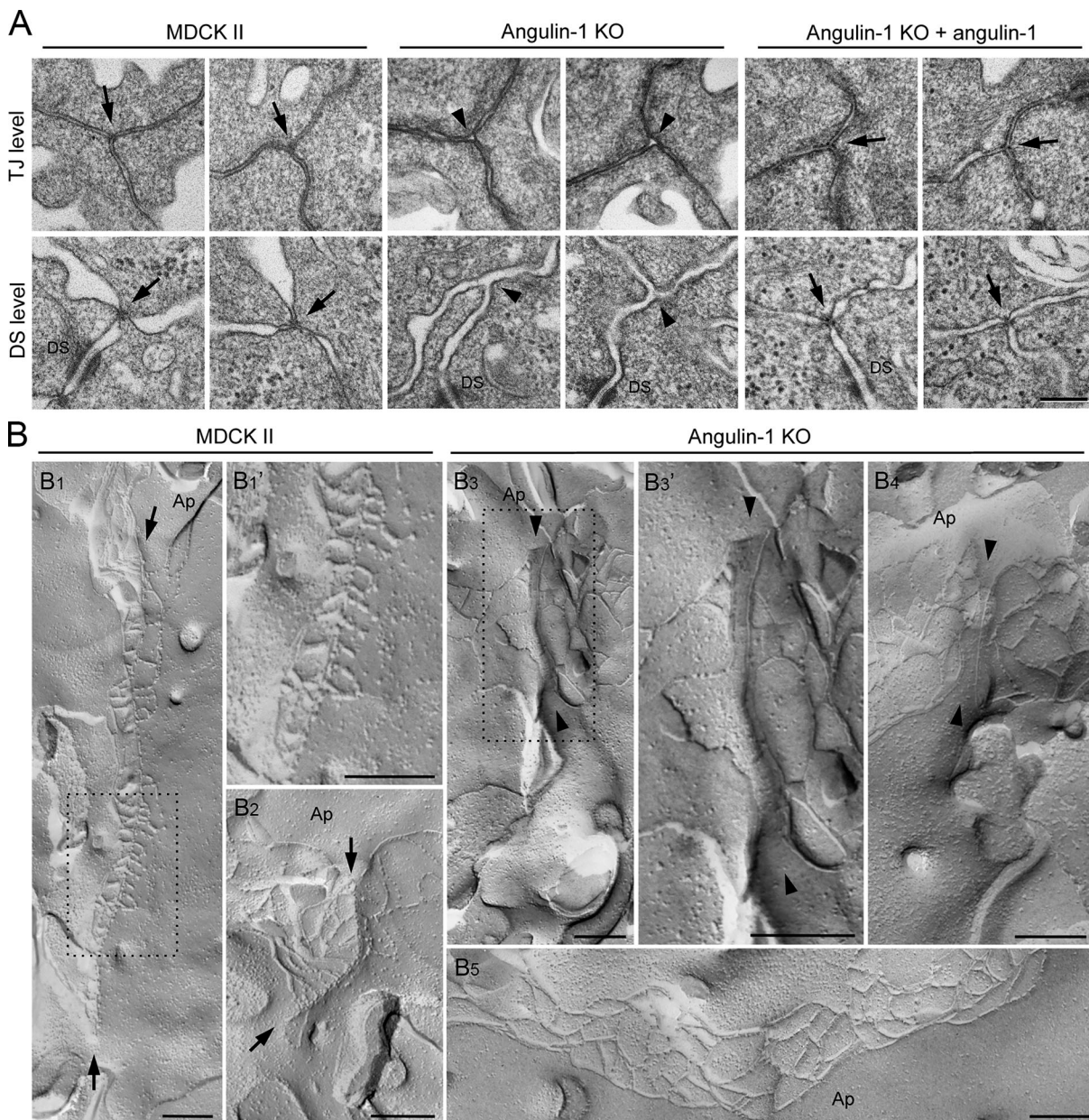


Figure 5. Aberrant ultrastructure of tTJs by depletion of angulin-1. (A) EM observation of horizontal ultrathin sections of MDCK II cells, angulin-1-KO cells, and angulin-1-KO cells expressing exogenous angulin-1 (angulin-1-KO + angulin-1). The three plasma membranes seal TCs at not only the level of TJs (TJ level) but also the more basal level of the lateral membrane containing desmosomes, but not TJs (DS level) in MDCK II cells and angulin-1-KO cells expressing exogenous angulin-1 (arrows). In contrast, apparent gaps are observed at TCs in angulin-1-KO cells (arrowheads). Two independent images are shown for TJ and DS levels of each cell type. Closed TCs/open TCs analyzed at the TJ level were 10/0 ($n = 10$) in MDCK II cells, 1/12 ($n = 13$) in angulin-1-KO cells, and 5/1 ($n = 6$) in angulin-1-KO cells expressing exogenous angulin-1. n indicates the number of observed TCs in which lipid bilayers of all of the three plasma membranes were recognized. DS, desmosome. (B) Freeze-fracture EM observation of TC regions in MDCK II cells and angulin-1-KO cells. In MDCK II cells (B₁, B₁' , and B₂), attached central sealing elements formed by vertical TJ strands are observed (between arrows) with variation in length depending on the TCs. B₁' is a magnified image of the boxed region in B₁. At TCs in angulin-1-KO cells (B₃, B₃' , and B₄), attached central sealing elements are not found, but vertical TJ strands separated by flat planes of the plasma membranes are observed (between arrowheads). B₃' is a magnified image of the boxed region in B₃. (B₅) Continuous TJ strands are observed at bicellular contacts in angulin-1-KO cells. Ap, apical side. Bars: 200 nm.

into ZO-1/ZO-2-dKO cells, both of the ZO-1 constructs were localized at cell-cell contacts in the apical region, while endogenous angulin-1 was localized at TCs and often extended along the apicobasal axis (Fig. S4, B-D). In the ZO-1-GFP-expressing cells, ZO-1-GFP colocalized with angulin-1 extending to the basal direction at TCs (Fig. S4 D). In contrast, in ZO-

1ΔPDZ2-GFP-expressing cells, ZO-1ΔPDZ2-GFP was localized only at the apical region, but it was not colocalized with angulin-1 at the lateral region at TCs (Fig. S4 D). In a pull-down assay using lysates of these cells, ZO-1-GFP bound to GST-ang575, but ZO-1ΔPDZ2-GFP did not (Fig. S4 E). These results suggest that the interaction between PDZ2 of ZO-1 and angulin-1 pbm is

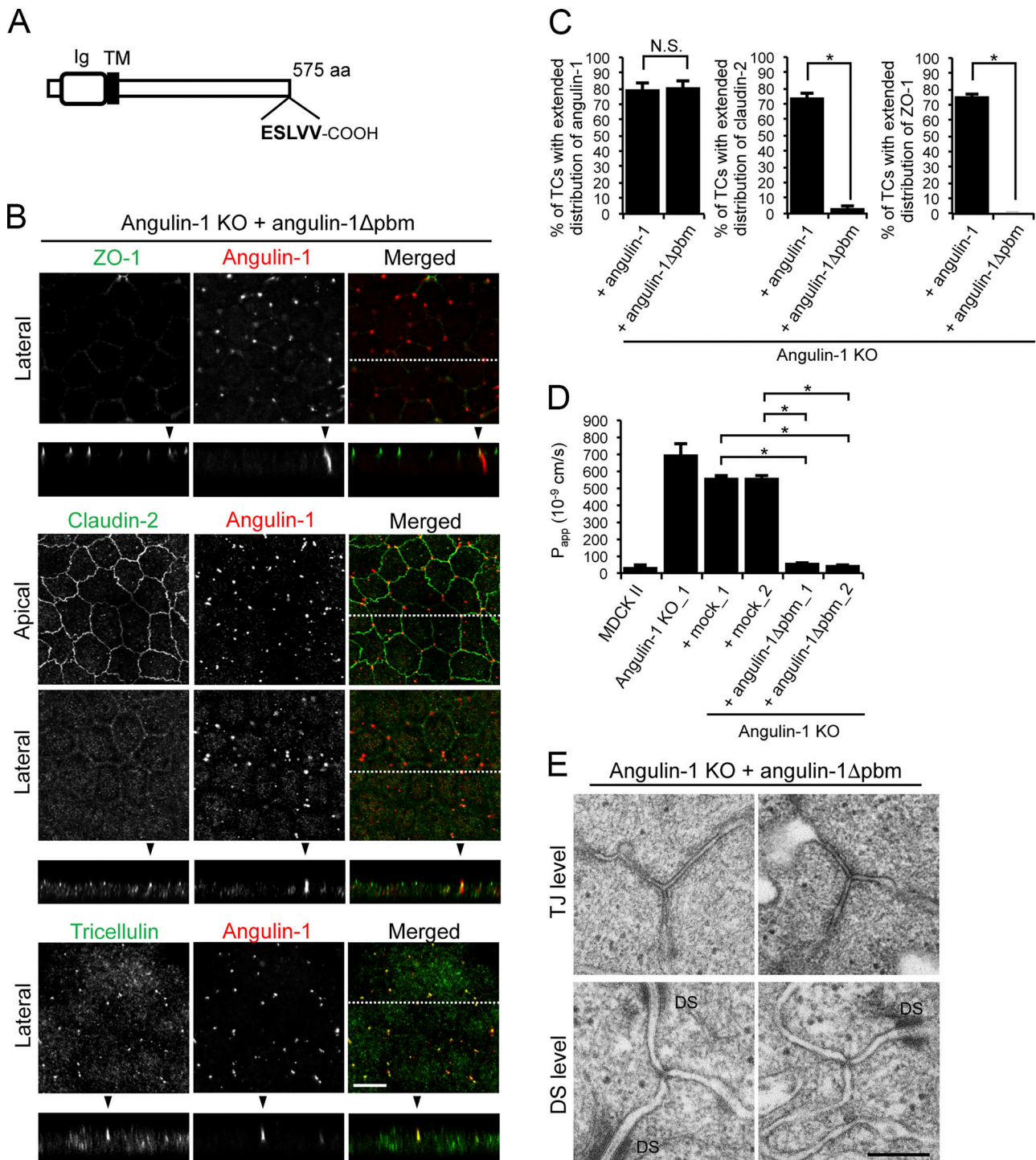


Figure 6. Role of the angulin-1 pbm in the localization of TJ proteins at TCs. (A) Schematic drawing of mouse angulin-1 with 575 amino acids. Five amino acids of the putative pbm at the C-terminus are shown. Ig, Ig-like domain; TM, transmembrane domain. (B) Double-immunofluorescence staining of angulin-1-KO cells expressing exogenous angulin-1 lacking the C-terminal five amino acids (angulin-1Δpbm) with anti-ZO-1 mAb and anti-angulin-1 mAb, anti-claudin-2 mAb and anti-angulin-1 mAb, or anti-tricellulin pAb and anti-angulin-1 mAb. Confocal sections of the apical region, including TJ markers and the lateral region, together with the corresponding Z-stack images along white dotted lines are shown. Arrowheads indicate TCs. Bar: 10 μm. (C) Quantification of TCs with extended distribution of fluorescence signals of angulin-1, claudin-2, and ZO-1 to the basal direction. The data in angulin-1-KO cells expressing angulin-1 (+ angulin-1) in the middle and right graphs are identical to those shown in Fig. 4 D. (D) Paracellular flux of fluorescein in MDCK II cells, angulin-1-KO cells, two independent mock-transfected angulin-1-KO cell clones (+mock_1 and +mock_2), and two independent angulin-1-KO cell clones expressing exogenous angulin-1Δpbm (+angulin-1Δpbm_1 and +angulin-1Δpbm_2). The data in MDCK II cells, angulin-1-KO cells, and two independent mock-transfected angulin-1-KO cell clones are identical to those in Fig. 4 F. P_{app} , apparent permeability. (E) EM observation of horizontal ultrathin sections of angulin-1-KO cells expressing exogenous angulin-1Δpbm. TCs at the level of TJs (TJ level) and the more basal level of the lateral membrane containing desmosomes (DS level) were analyzed. Two independent images are shown for TJ and DS levels. Closed TCs/open TCs analyzed at the TJ level were 2/0 ($n = 2$). DS, desmosome. Bar: 200 nm. (C and D) Data are shown as mean ± SD ($n = 3$) and were analyzed by the Tukey-Kramer test. *, $P < 0.01$.

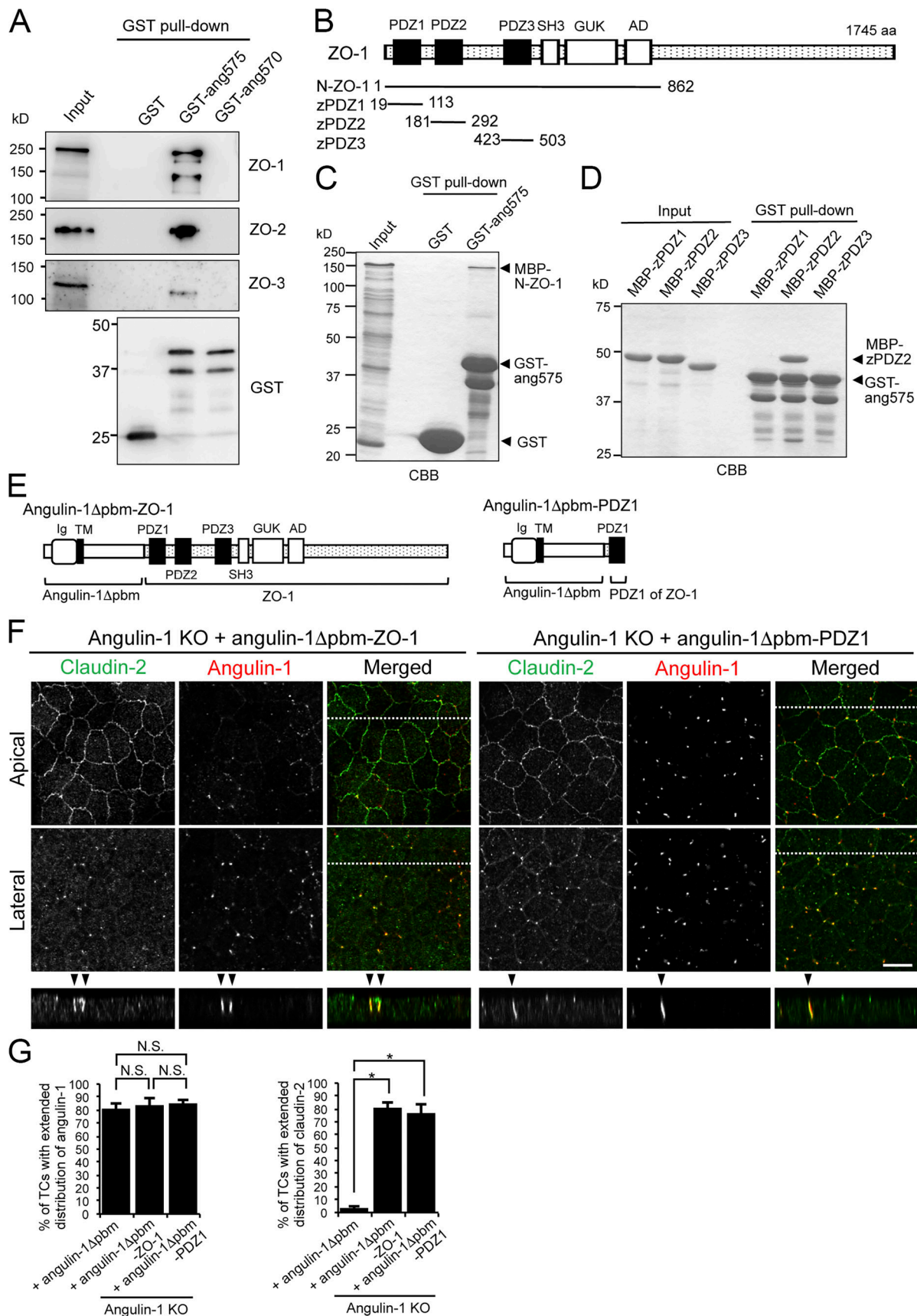


Figure 7. **Direct binding of the angulin-1 pbm to ZO-1 and its role in tTJ formation.** (A) Lysates of angulin-1-KO cells were incubated with GST and GST fusion proteins of aa 409–575 and aa 409–570 of angulin-1 (GST-ang575 and GST-ang570, respectively) and subjected to GST pull-down assays. The lysates

(input) and precipitates with GST, GST-ang575, and GST-ang570 were analyzed by Western blotting with anti-ZO-1 mAb, anti-ZO-2 pAb, and anti-ZO-3 pAb. The precipitates were also immunoblotted with anti-GST pAb. **(B)** Schematic diagram of the domain structure of mouse ZO-1 protein with 1,745 amino acids. ZO-1 contains three PDZ domains, an SH3 domain, a guanylate kinase domain (GUK), and an acidic domain (AD) in its N-terminal half. Four distinct portions of ZO-1 indicated as solid lines with amino acid numbers were produced as recombinant fusion proteins with MBP. **(C)** GST pull-down assays of MBP-N-ZO-1 fusion protein with GST-ang575. Input: crude lysate of *Escherichia coli* expressing MBP-N-ZO-1. **(D)** GST pull-down assays of MBP fusion proteins of PDZ1, PDZ2, and PDZ3 of ZO-1 (MBP-zPDZ1, MBP-zPDZ2, and MBP-zPDZ3, respectively) with GST-ang575. Input: each MBP fusion protein. In C and D, the samples were subjected to SDS-PAGE followed by Coomassie Brilliant Blue (CBB) staining. **(E)** Schematic diagram of a chimeric protein of angulin-1Δpbm with full-length ZO-1 (angulin-1Δpbm-ZO-1) and a chimeric protein of angulin-1Δpbm with PDZ1 domain of ZO-1 (angulin-1Δpbm-PDZ1). **(F)** Angulin-1-KO cells expressing angulin-1Δpbm-ZO-1 or angulin-1Δpbm-PDZ1 were immunostained with anti-angulin-1 mAb and anti-claudin-2 mAb. Confocal sections of the apical region, including claudin-2 staining and the lateral region, together with the corresponding Z-stack images along the white dotted lines are shown. Arrowheads indicate TCs. Bar: 10 μm. **(G)** Quantification of TCs with extended distribution of fluorescence signals of angulin-1 chimeras and claudin-2 to the basal direction. The data in angulin-1-KO cells expressing angulin-1Δpbm (+ angulin-1Δpbm) in the left and right graphs are identical to those in Fig. 6 C. Data are shown as mean ± SD (n = 3) and were analyzed by the Tukey-Kramer test. *, P < 0.01.

required for the extended localization of ZO-1 along the apicobasal axis.

To confirm the role of the binding between angulin-1 and ZO-1 in the localization of TJ proteins at TCs, we expressed a chimeric protein of angulin-1Δpbm and full-length ZO-1 (angulin-1Δpbm-ZO-1) in angulin-1-KO cells (Fig. 7 E and Fig. S2 D). Immunofluorescence staining of stable transfectants with an anti-angulin-1 pAb showed vertically extended localizations of angulin-1Δpbm-ZO-1 (Fig. 7, F and G). Moreover, claudin-2 was colocalized with angulin-1Δpbm-ZO-1 along the apicobasal axis at TCs (Fig. 7, F and G), different from the case with angulin-1Δpbm (Fig. 6, B and C). The same results were obtained when a chimeric protein of angulin-1Δpbm and the PDZ1 domain of ZO-1 (angulin-1Δpbm-PDZ1) was expressed in angulin-1-KO cells (Fig. 7, E–G; and Fig. S2 D). These results suggest that the ZO-1 binding to angulin-1 supports the extended localization of claudin-2 along the apicobasal axis at TCs via its PDZ1 domain.

The plasma membrane contact at TCs occurs independently of claudins and JAM-A

Angulin-1Δpbm showed extended localization along the apicobasal axis unaccompanied by claudin-2 when expressed in angulin-1-KO cells (Fig. 6, B and C), but it was able to seal the extracellular space at TCs. This suggests that angulin-1 may form the plasma membrane contact at TCs without claudins. To examine this possibility, we analyzed the morphology of TCs in claudin-based TJ strand-deficient epithelial cells, which we recently established by genome editing-based disruption of claudin-1, -2, -3, -4, and -7 genes in MDCK II cells (claudin-quinKO cells; Otani et al., 2019). Claudin-quinKO cells lack TJ strands but retain JAM-A-mediated plasma membrane appositions with ~6–7-nm distance at the apical-junctional complex (AJC) level (Otani et al., 2019). Immunofluorescence staining revealed that angulin-1 was localized at TCs and bicellular contacts in the apical region in claudin-quinKO cells. Angulin-1 was also detected along bicellular contacts diffusely in the lateral region (Fig. 8 A). EM observation of horizontal ultrathin sections revealed that the extracellular space between the three plasma membranes at TCs was obliterated in claudin-quinKO cells at the apical cell–cell junction level with plasma membrane appositions (Fig. 8 B). The plasma membrane contact at TCs was also found in horizontal sections containing desmosomes (Fig. 8 B). To confirm that the plasma membrane contact at TCs in claudin-quinKO cells is mediated by angulin-1, we established angulin-

1-KO cells in a claudin-quinKO background (claudin/angulin-1-KO; Figs. 8 C and S5 A). The three claudin/angulin-1-KO cell clones showed increased paracellular flux of 150 kD FITC-dextran compared with three control clones (Fig. 8 D). Furthermore, an apparent gap was observed at TCs in claudin/angulin-1-KO cells (Fig. 8 E). To examine the requirement of JAM-A-mediated membrane appositions for angulin-1 assembly and plasma membrane contact formation at TCs, we analyzed claudin/JAM-A-KO cells established from claudin-quinKO cells by disrupting the JAM-A gene (Otani et al., 2019). In claudin/JAM-A-KO cells, angulin-1 signals were clearly detected at TCs as well as bicellular contacts at the level of apical junctions on immunofluorescence (Fig. 8 F). Western blot analyses revealed that the angulin-1 level increased both in claudin-quinKO cells and in claudin/JAM-A-KO cells due to an unknown reason and that this might cause the spread of angulin-1 into bicellular contacts (Fig. S2 E). Because angulin-1 localization at bicellular contacts in the apical region in claudin/JAM-A-KO cells was more remarkable than in claudin-quinKO cells, we investigated a possible competition between angulin-1 and JAM-A in the localization at bicellular contacts. However, we could not find any remarkable difference of angulin-1 localization in JAM-A-KO cells, while JAM-A localization appeared normal in angulin-1-KO cells (Fig. S2, F and G). On EM of horizontal ultrathin sections of claudin/JAM-A-KO cells, the plasma membrane contact at TCs was clearly observed in sections of the apical cell–cell junction level containing parallel plasma membranes with a narrow space. The plasma membrane contact was also observed in sections containing desmosomes (Fig. 8 G).

These results demonstrate that neither claudin-based TJ strands nor JAM-A-mediated membrane appositions are required for the angulin-1-mediated plasma membrane contact at TCs.

Tricellulin is required for connection of TJ strands to the central sealing elements, but not for epithelial barrier function

Considering that angulins recruit tricellulin to TCs, the angulin-1-mediated plasma membrane contact at TCs may be attributed to tricellulin. To examine this idea, we established four independent tricellulin-deficient cell clones from MDCK II cells using CRISPR/Cas9-mediated genome editing (Fig. 9, A and B; and Fig. S5 B). Tricellulin contains four transmembrane domains, N- and C-terminal cytoplasmic domains, two extracellular loops, and a short cytoplasmic turn. The obtained tricellulin-KO cell clones may allow expression of the N-terminal half of tricellulin with a

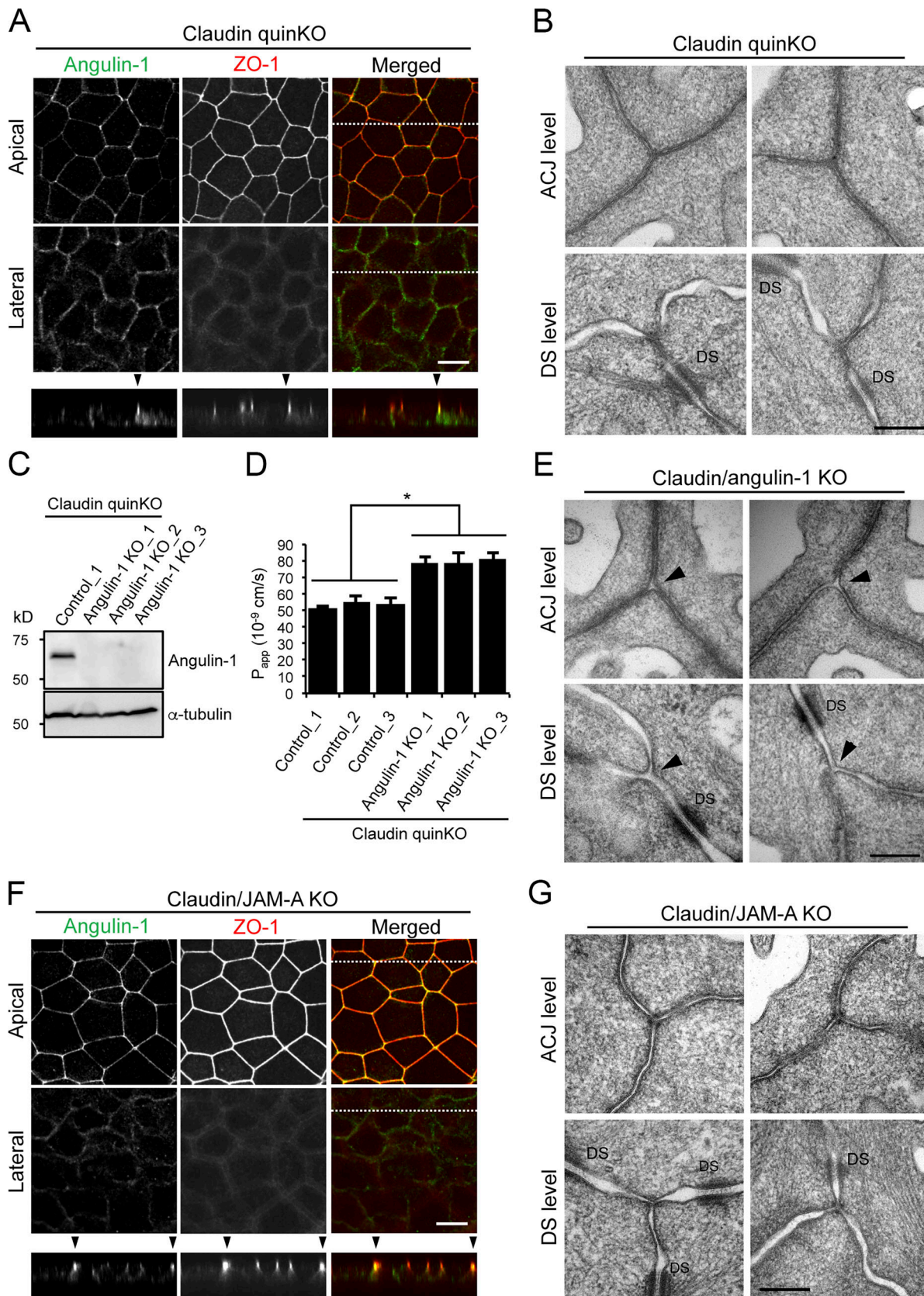


Figure 8. **The plasma membrane contact at TCs is maintained in claudin-quinoKO cells and claudin/JAM-A-KO cells.** (A) Immunofluorescence staining of claudin-quinoKO cells with anti-angulin-1 pAb and anti-ZO-1 mAb. (B) EM observation of horizontal ultrathin sections of claudin-quinoKO cells. (C) Western blotting of lysates of a control clone of claudin-quinoKO cells and three clones of angulin-1-KO cells in claudin-quinoKO background (claudin/angulin-1-KO cells) with anti-angulin-1 pAb or anti- α -tubulin mAb. (D) Paracellular flux of 150 kD FITC-dextran in control clones of claudin-quinoKO cells and claudin/angulin-1-KO

cell clones. Data are shown as mean \pm SD ($n = 3$) and were analyzed by Student's *t* test ($n = 9$ total for three control clones [$n = 3$ per clone] versus $n = 9$ total for three claudin/angulin-1-KO clones [$n = 3$ per clone]). *, $P < 0.01$. P_{app} , apparent permeability. **(E)** EM observation of horizontal ultrathin sections of claudin/angulin-1-KO cells. **(F)** Immunofluorescence staining of claudin/JAM-A-KO cells with anti-angulin-1 pAb and anti-ZO-1 mAb. **(G)** EM observation of horizontal ultrathin sections of claudin/JAM-A-KO cells. In A and F, confocal sections of the apical region, including ZO-1 staining and the lateral region, together with the corresponding Z-stack images along the white dotted lines are shown. In both cells, intense signals for angulin-1 at TCs were limited to the apical region and did not extend to the basal direction. Arrowheads indicate TCs. Bars: 10 μ m. In B, E, and G, TCs at the level of apical cell-cell junctions without desmosomes (ACJ level) and the more basal level of the lateral membrane containing desmosomes (DS level) were analyzed. Two independent images are shown for both levels of each cell type. Closed TCs/open TCs at the ACJ level were 7/1 ($n = 8$) in claudin-quinKO cells, 1/7 ($n = 8$) in claudin/angulin-1-KO cells, and 9/0 ($n = 9$) in claudin-quin/JAM-A-KO cells. Note that the intercellular space is widened in the apical region of claudin/JAM-A-KO cells. DS, desmosome. Bars: 200 nm.

frameshift around aa 275, located at the cytoplasmic turn between the second and third transmembrane domains. However, no signals for truncated tricellulin at TCs were detected in these cells by immunofluorescence staining with an antibody against the N-terminal cytoplasmic region of tricellulin (Fig. 9 B), indicating that tricellulin was functionally impaired. Immunofluorescence staining of tricellulin-KO cells revealed that angulin-1 was localized at TCs with apicobasal extension and colocalized with claudin-2 (Fig. 9, C and D). ZO-1 was mostly colocalized with angulin-1 along the apicobasal axis at TCs, but it was infrequently missing from some angulin-1 rods (Fig. 9, C and E). Unlike angulin-1-KO cells (Fig. 4 E), all four tricellulin-KO cell clones showed no increase in paracellular flux of fluorescein compared with MDCK II cells (Fig. 9 F). Moreover, alterations in TER and paracellular flux of fluorescein were not detected in tricellulin-KO cells on a claudin-2-KO background (Fig. S5, C-F). Finally, we analyzed the TC ultrastructure in tricellulin-KO cells by EM. Horizontal ultrathin sections at the TJ level revealed that tricellulin-KO cells contained either the plasma membrane contact or a gap at TCs (Fig. 9 G). The plasma membrane contact at TCs was also observed at the desmosome level in tricellulin-KO cells (Fig. 9 G). On freeze-fracture replica EM, the central sealing elements with apicobasal extension were observed at TCs in tricellulin-KO cells. Intriguingly, however, there were hardly any connections of short TJ strands to the central sealing elements (Fig. 9, H₁, H₁', H₂, and H₃; and Fig. S5 G). At some TCs, apical TJ strands from both sides appeared to cave in and attach to one another to form central sealing elements that extended in the basal direction (Fig. 9 H₃). The cave-in of TJ strands likely corresponded to the gap at TCs at the TJ level observed in horizontal ultrathin sections (Fig. 9 G). These observations suggest that tricellulin is required for the organization of tTJs by connecting short TJ strands to the central sealing elements but is not essential for the formation of the central sealing elements, plasma membrane contact at TCs, or the epithelial barrier function.

Discussion

In the present study, we examined the roles of angulin-1 and tricellulin in tTJ formation and epithelial barrier function in MDCK II cells by loss-of-function analyses using genome editing. We found that angulin-1 is required for the plasma membrane contact at TCs, central sealing element formation, and epithelial barrier function, while tricellulin is not (Fig. 10). We also found that claudin-based TJ strands are dispensable for the plasma membrane contact at TCs. These results suggest that angulin family proteins are essential for the plasma membrane seal at

TCs, which should be a key step in tTJ formation, independently of tricellulin and claudins.

Apicobasal extension of tTJs

We found that tTJ proteins, including tricellulin and angulin family proteins, extended along the apicobasal axis at TCs in epithelial cells in mouse tissues and MDCK II cells by immunofluorescence microscopy. Because tricellulin and angulin-1 are localized along the central sealing elements of tTJs on freeze-fracture immunolabeling EM (Ikenouchi et al., 2005; Masuda et al., 2011), it is reasonable that the rodlike fluorescent signals of tTJ proteins reflect the outline of tTJs by light microscopy. In mouse proximal tubules, tricellulin and angulin-1 signals were visualized as dots rather than as rods, suggesting that the extent of the apicobasal extension of tTJs depends on epithelial cell types. It was reported that TJs at bicellular contacts in proximal tubules contain one or two TJ strands, while those in collecting ducts contain approximately seven TJ strands (Claude and Goodenough, 1973). The thickness of TJs may influence the depth of tTJs along the apicobasal axis. Importantly, claudins, occludin, and ZO-1 were distributed along the apicobasal axis at TCs and colocalized with tricellulin and angulins, suggesting that TJ-associated proteins are also incorporated into tTJs. Ikenouchi et al. (2005) reported that tricellulin was detected as vertically oriented rods at TCs, while occludin was concentrated as dots at the most apical region of the tricellulin rods in Z-stack confocal sections of mouse EpH4 mammary epithelial cells evaluated by immunofluorescence. These descriptions cannot exclude the existence of occludin in tTJs, because the TJ-to-tTJ ratio of occludin may vary depending on cell types. Considering the limitations of light microscopy, it is difficult to clarify whether these TJ-associated proteins are localized at the central sealing elements and/or short TJ strands connected to the central sealing elements within tTJs by immunofluorescence staining. In tricellulin-KO cells, the central sealing elements, which closely resemble TJ strands, were observed in tTJs by freeze-fracture EM, and claudin-2 was colocalized with angulin-1 along the apicobasal axis at TCs by immunofluorescence staining. These observations suggest that claudins are incorporated into the central sealing elements of tTJs. Further investigations by super-resolution microscopy or freeze-fracture immunolabeling EM are needed to reveal the precise distributions of TJ-associated proteins within tTJs.

In addition to TJ proteins, we have shown that α -catenin under tension and afadin were localized along the apicobasal axis at TCs in MDCK II cells, suggesting that AJs occur along tTJs at TCs. The role of AJs at TCs is of interest in terms of dynamic behavior of epithelial cells. TCs appear to support tensile force of

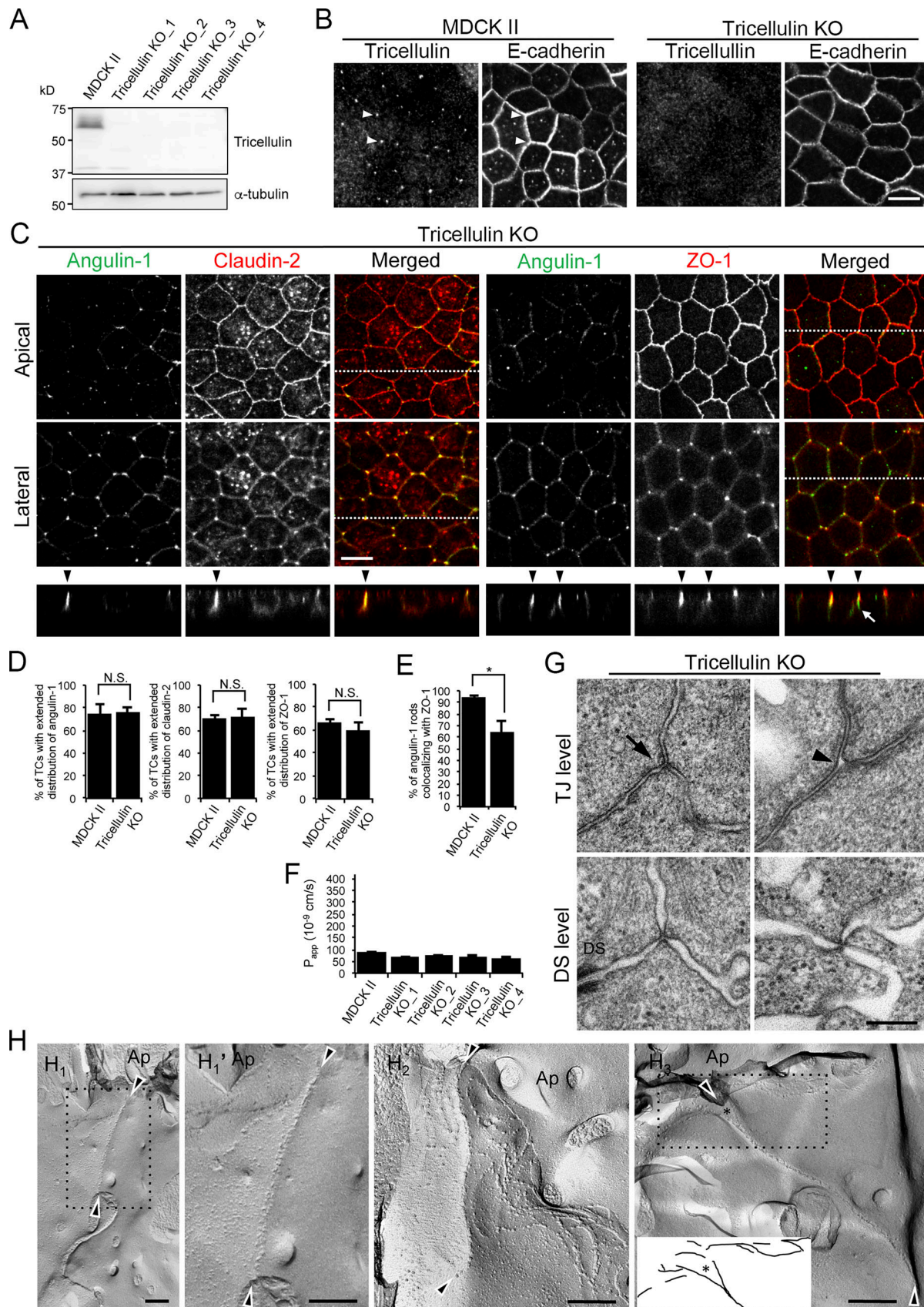


Figure 9. **Roles of tricellulin in tTJ formation and epithelial barrier function.** (A) Lysates of four independent tricellulin-KO cell clones (tricellulin-KO_1-4) were analyzed by Western blotting with anti-tricellulin pAb or anti- α -tubulin mAb. (B) Tricellulin-KO_4 cells were immunostained with anti-tricellulin pAb and

anti-E-cadherin mAb. Arrowheads indicate TCs. **(C)** Double-immunofluorescence staining of tricellulin-KO_4 cells with anti-angulin-1 pAb and anti-claudin-2 mAb or anti-angulin-1 pAb and anti-ZO-1 mAb. Arrowheads indicate TCs. Confocal sections of the apical region, including TJ markers and the lateral region, together with the corresponding Z-stack images along the white dotted lines are shown. The white arrow indicates an angulin-1-positive region at a TC without ZO-1. **(D)** Quantification of TCs with extended distribution of fluorescence signals of angulin-1, claudin-2, and ZO-1 to the basal direction. The data in MDCK II cells in the middle and right graphs are identical to those in Fig. 4 D. **(E)** Quantification of angulin-1 rods colocalizing with ZO-1 at TCs. **(F)** Paracellular flux of fluorescein in MDCK II and tricellulin-KO_1-4 cells. Data are shown as mean \pm SD ($n = 3$). P_{app} , apparent permeability. **(G)** EM observation of horizontal ultrathin sections of tricellulin-KO_4 cells. TCs at the level of TJs (TJ level) and the more basal level of the lateral membrane containing desmosomes (DS level) were analyzed. The TJ level contained either the plasma membrane contact (arrow) or a gap (arrowhead) at TCs. The number of closed TCs/open TCs analyzed at the TJ level was 2/4 ($n = 6$). Close plasma membrane contacts at TCs were also observed at the DS level. **(H)** Freeze-fracture EM observation of tricellulin-KO_4 cells. Arrowheads indicate the central sealing elements without connection of short TJ strands (H_1 , H_1' , H_2 , and H_3). In H_3 , visible TJ strands in the dotted box are traced. The asterisk indicates a cave-in of vertical TJ strands. Ap, apical side. **(D and E)** Data are shown as mean \pm SD ($n = 3$) and were analyzed by Student's *t* test. *, $P < 0.01$. Bars: 10 μm (B and C) and 200 nm (E and F).

actomyosin along AJs (Honda, 1983; Cavey and Lecuit, 2009). Changes in the length of cell-cell junctions observed in cell rearrangement should accompany dynamic reorganization of TCs, leading to the idea that TCs are regulatory units of epithelial remodeling (Cavey and Lecuit, 2009). In *Drosophila*, a tricellular AJ component, Sidekick, has been shown to be involved in dynamic remodeling of epithelial cells (Letizia et al., 2019; Uechi and Kuranaga, 2019; Finegan et al., 2019). However, little is known about the organization and roles of tricellular AJs in vertebrate cells. Many issues about tricellular AJs should be investigated in the future, including their detailed distribution, possible dependency on tTJs, and roles in actomyosin organization at TCs.

Roles of ZO-1 binding to angulin-1 in claudin localization at TCs

We found that the pbm in the angulin-1 C-terminus directly binds to PDZ2 of ZO-1. Angulin-1 Δ pbm was distributed along the

apicobasal axis at TCs similar to the full-length angulin-1 and colocalized with tricellulin, but not ZO-1 and claudins when expressed in angulin-1-KO cells. However, forced conjunction of the full-length ZO-1 or its PDZ1 domain to angulin-1 Δ pbm induced apicobasal extension of claudins at TCs. These results suggest that ZO-1 mediates claudin recruitment to angulin-1 along the apicobasal axis through its PDZ1 domain, which directly binds to the C-terminal pbm of claudins (Itoh et al., 1999). However, the real molecular mechanism for TJ protein assembly in tTJs appears more complex. In tricellulin-KO cells, claudin-2 was colocalized with angulin-1 along the apicobasal axis at TCs. Consistently, the central sealing elements were observed in these cells by freeze-fracture EM. However, ZO-1 was incompletely colocalized with angulin-1 along the apicobasal axis at TCs in tricellulin-KO cells. These observations indicate that tricellulin is involved in the colocalization of ZO-1 with angulin-1

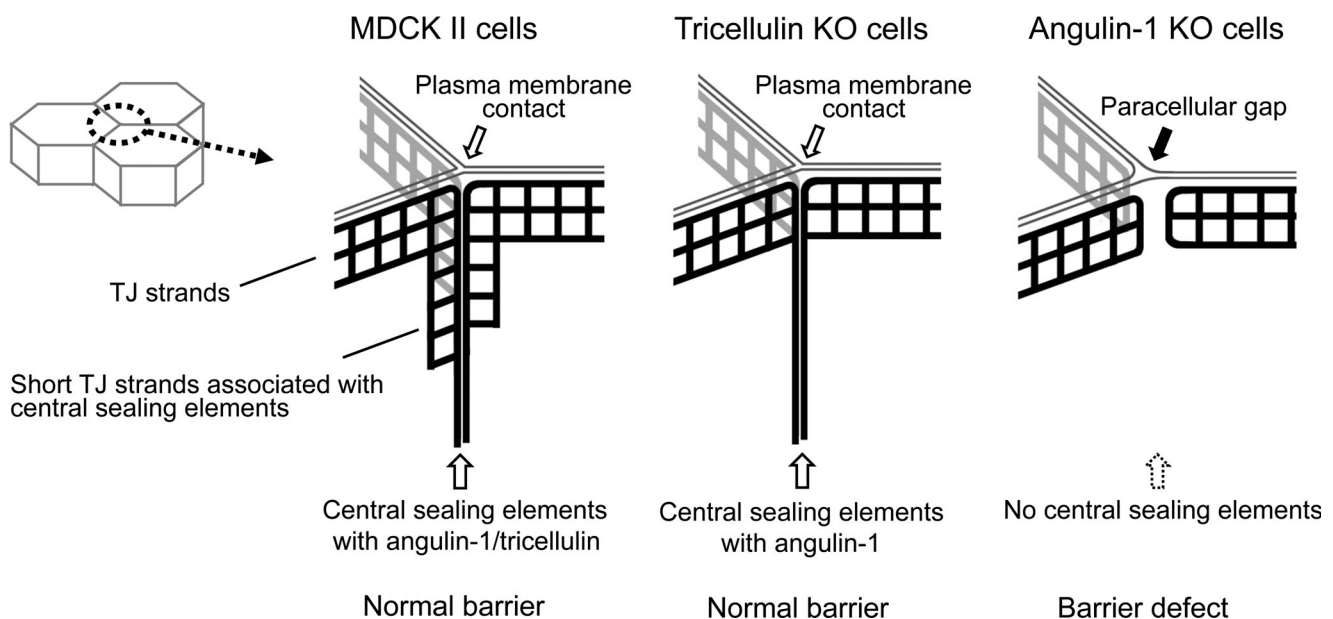


Figure 10. Summary of the phenotypes of MDCK II, angulin-1-KO, and tricellulin-KO cells for tTJ formation and epithelial barrier function. In MDCK II cells, angulin-1 and tricellulin were localized at TCs extending along the apicobasal axis. The plasma membrane contact at TCs was observed in horizontal ultrathin sections. In freeze-fracture replicas, typical tTJs containing the central sealing elements and associated short TJ strands were observed. In tricellulin-KO cells, angulin-1 was localized at TCs extending along the apicobasal axis. The plasma membrane contact and the central sealing elements were maintained, but the central sealing elements lacked connection of short TJ strands. In angulin-1-KO cells, a paracellular gap was observed at TCs in horizontal ultrathin sections. In freeze-fracture replicas, the vertical TJ strands at TCs were separated and did not form the central sealing elements. The epithelial barrier function was impaired in angulin-1-KO cells, but not in tricellulin-KO cells.

and that ZO-1 is not the only determinant for colocalization of claudins with angulin-1. Riazuddin et al. (2006) observed direct binding of the N-terminal half of ZO-1 to the C-terminal cytoplasmic domain of tricellulin by in vitro binding assays. Meanwhile, Ikenouchi et al. (2008) showed that a claudin-3 mutant lacking the C-terminal pbm and tricellulin was highly colocalized at cell–cell contacts when overexpressed in mouse L fibroblasts without recruiting ZO-1, suggesting an interaction between claudins and tricellulin in the plasma membrane, regardless of ZO-1. It was also shown that claudins lacking the C-terminal pbm can polymerize in the plasma membrane to form TJ strand-like structures in mouse L fibroblasts (Furuse et al., 1999; Ikenouchi et al., 2008), suggesting an intrinsic ability of claudins for TJ strand formation at least under certain conditions. These molecular interactions may cooperatively regulate the recruitment of claudins to angulin-1-positive regions at TCs to form tTJs.

Roles of angulins in the plasma membrane contact at TCs

As the most important finding in this study, we demonstrated that angulin-1 is involved in the plasma membrane contact at TCs to obliterate the paracellular space. The plasma membrane contact at TCs was disrupted in angulin-1-KO cells but was maintained in tricellulin-KO cells. Moreover, the plasma membrane contact at TCs was observed in not only claudin-quinKO cells lacking claudin-based TJ strands but also claudin/JAM-A-KO cells lacking JAM-A-mediated plasma membrane appositions. Angulin-1Δpbm, which lacks ZO-1-binding ability, generated the plasma membrane contacts at TCs when expressed in angulin-1-KO cells. Taken together, angulin-1 is responsible for the plasma membrane contact at TCs independently of tricellulin, claudins, JAM-A, and binding to ZO-1. In claudin-quinKO cells and claudin/JAM-A-KO cells, angulin-1 was localized at the level of the AJC but was mostly absent at the level of the lateral membrane. However, the plasma membrane contact at TCs in EM was observed even at the desmosome level. In these cells, angulin-1 may extend basally to some extent, which is hardly detectable by confocal microscopy with poor z axis resolution. The depth of the plasma membrane contact at TCs in these cells requires further clarification by serial ultrathin section analyses.

In angulin-1-KO cells, the reduction in epithelial barrier function corresponded to gap formation at the paracellular space of TCs, while continuous TJ strands at bicellular contacts were observed in freeze-fracture replicas. These observations indicate that angulin-1-mediated obliteration of the paracellular space at TCs is crucial for the full barrier function of epithelial cellular sheets. Interestingly, angulin-1Δpbm rescued the epithelial barrier function in angulin-1-KO cells or angulin-1/claudin-2-dKO cells to a similar level of the full-length angulin-1. This suggests that the recruitment of claudins along the apicobasal axis may not be essential for the angulin-1-mediated paracellular barrier at TCs. It is necessary to establish whether angulin-2 and angulin-3 can generate the plasma membrane contact at TCs and the central sealing elements at tTJs. If these proteins can reconstitute tTJs in angulin-1-KO cells similar to angulin-1, it will be of interest to clarify the functional differences among the angulin subtypes.

Regarding the mechanism behind angulin-1 assembly at TCs, we recently showed that both dense cytoplasmic palmitoylation and the extracellular domain of angulin-1 are required for its TC localization (Oda et al., 2020). We proposed that the highly palmitoylated cytoplasmic domain of angulin-1 has weak affinity with a cholesterol-mediated membrane domain at TCs with high curvature convex to the outside (Oda et al., 2020), while the extracellular domain has a weak homophilic interaction (Masuda et al., 2011). Using both properties, angulin-1 may autonomously assemble into TCs, namely cell–cell contact sites with high curvature convex to the outside (Oda et al., 2020). Considering that JAM-A with two Ig-like domains in its extracellular region generates very close membrane appositions with only 6–7-nm distance (Otani et al., 2019), it may be reasonable that angulin-1 with a single Ig-like domain can form the plasma membrane contact at TCs with almost no extracellular space. Recently, giant unilamellar vesicles containing reconstituted claudin-4 were shown to form adhesive membrane interfaces with a fence function against extracellular membrane proteins (Belardi et al., 2018). In these vesicles, close membrane contacts were absent at trivesicular junctions, indicating that claudins are not sufficient for tTJ formation. It will be interesting to examine whether angulins can cross-link trivesicular junctions using this simple reconstitution system in which the lipid content can be controlled to understand the mechanism for angulin-mediated membrane contact formation at TCs.

Continuous bicellular TJs were retained in angulin-1-KO cells, while angulin-1 sealed TCs but was spread to bicellular contacts in claudin-quinKO cells and claudin/JAM-A-KO cells. These observations indicate that the basic mechanisms for bicellular TJ formation and tTJ formation are independent of one another but are coordinately organized in epithelial cells to form a functional paracellular barrier. Interestingly, a similar feature is known in *Drosophila* septate junctions (SJs) and tricellular junctions (TCJs), although molecular components of tTJs and *Drosophila* TCJs are not conserved (Byri et al., 2015; Schulte et al., 2003; Dunn et al., 2018). The lack of Aka or M6 hampers TCJ formation but not SJ formation, while Aka can localize to TCJ in mutants lacking SJs, suggesting that the assembly of TCJs and SJs is independently operated (Byri et al., 2015; Wittek et al., 2020; Esmangart de Bournonville and Le Borgne, 2020). However, TCJs and SJs influence each other around cell vertices because Aka is required for the anchoring of SJ components at TCJs and, vice versa, loss of SJ integrity leads to TCJ components to spread to bicellular contacts (Esmangart de Bournonville and Le Borgne, 2020).

Roles of tricellulin in tTJ formation

In our study, the plasma membrane contact at TCs and epithelial barrier function were retained in tricellulin-KO cells. Thus, the question arises as to the role of tricellulin in tTJs. In freeze-fracture EM, tricellulin-KO cells had basally extended central sealing elements at TCs but lost short TJ strands connected to the central sealing elements. Similar structural defects in tTJs were observed in hair cells in utricular macula in the inner ear of *Tric^{R497X/R497X}* mice, which mimic a mutation in the human tricellulin-encoding gene causing hearing loss (Nayak et al.,

2013). These observations indicate that tricellulin is required for the connection of short TJ strands to the central sealing elements of tTJs. Consistent with this notion, tricellulin expression reconstituted by claudin-1 in mouse L fibroblasts (Ikenouchi et al., 2008) and HEK293 cells (Cording et al., 2013), resulting in the formation of compressed TJ strand meshworks. Consistently, it has been reported recently that tricellulin and occludin play a role in the formation of an anastomosing TJ strand network in MDCK II cells (Saito et al., 2021). However, the mechanism by which tricellulin induces end-to-side connections of TJ strands remains elusive. We previously showed that the N-terminal cytoplasmic domain of tricellulin binds to the Cdc42 guanine nucleotide exchange factor Tuba, activates Cdc42, and regulates F-actin organization during cell-cell junction formation in cultured epithelial cells (Oda et al., 2014). It will be of interest to elucidate how tricellulin regulates juxtamembrane F-actin organization at TCs through Cdc42 activation and whether this action of tricellulin influences end-to-side connections of TJ strands. Alternatively, tricellulin may mediate end-to-side connections of TJ strands as a joint. Recently, Van Itallie et al. (2017) showed that occludin tends to concentrate at TJ strand ends and end-to-side junction points of TJ strands in Rat-1 fibroblasts expressing claudins and occludin (Van Itallie et al., 2017). Considering that tricellulin shares structural similarity with occludin (Ikenouchi et al., 2005), tricellulin may concentrate at the junctions of TJ strands and facilitate their branching.

Despite the loss of short TJ strands in the vicinity of the central sealing elements, we did not detect any impairment of the epithelial barrier function in tricellulin-KO cells by conventional barrier assays. This suggests that tricellulin has a subtle role in the epithelial barrier function. It was reported that RNAi-mediated suppression of tricellulin decreased TER and increased paracellular flux in mouse EpH4 mammary epithelial cells (Ikenouchi et al., 2005), while overexpression of tricellulin reduced paracellular flux in MDCK II cells (Krug et al., 2009). The discrepancy between these previous studies and the present study may arise from differences in the cells or experimental conditions used. It should be noted in *Tric^{R497X/R497X}* mice that, different from hair cells in utricular macula, the pair of central sealing elements were split in inner hair cells in the organ of Corti in a freeze-fracture replica, suggesting a possibility that the impact of tricellulin may differ depending on cell types (Nayak et al., 2013). Meanwhile, the notion of a subtle role for tricellulin in the epithelial barrier function appears consistent with the results of *in vivo* loss-of-function studies on tricellulin. No significant decreases in endocochlear potential were observed in *Tric^{R497X/R497X}* mice and tricellulin-KO mice, although the mice showed progressive hearing loss associated with hair cell degeneration (Nayak et al., 2013; Kamitani et al., 2015). In *Tric^{R497X/R497X}* mice and tricellulin-KO mice, a biotin-based tracer did not permeate from the perilymph to the stria vascularis (Nayak et al., 2013; Kamitani et al., 2015). Furthermore, although tricellulin is ubiquitously expressed in epithelial tissues, no other clinical manifestations were cosegregated with hearing loss in two DFNB49 families with tricellulin mutations

(Nayak et al., 2015). In contrast, the phenotypes caused by angulin deficiencies are diverse and severe. Angulin-1-deficient mice exhibit embryonic lethality with blood-brain barrier failure (Mesli et al., 2004; Sohet et al., 2015), while angulin-2-deficient mice show polyuria and polydipsia arising from renal concentrating defects in addition to hearing loss (Higashi et al., 2015; Morozko et al., 2015; Sang et al., 2015; Gong et al., 2017). Recently, mutations in the angulin-1 gene have been reported in patients with infantile intrahepatic cholestasis (Uehara et al., 2020; Maddirevula et al., 2019). These lines of evidence support the idea that angulins, but not tricellulin, play essential roles in the plasma membrane seal at TCs and in epithelial barrier function.

Materials and methods

Cell culture and antibodies

MDCK II cells were provided by Dr. Masayuki Murata (University of Tokyo, Tokyo, Japan). ZO-1/ZO-2-dKO cells, claudin-quinKO cells, claudin/JAM-A-KO cells, and JAM-A-KO cells were established as described previously (Otani et al., 2019). Cells were grown in DMEM (low glucose, 05919; Nissui) supplemented with 10% FBS. Rat anti-tricellulin mAb (C96; Ikenouchi et al., 2005), rat anti-occludin mAb (Saitou et al., 1997), rabbit anti-angulin-1 pAb (Oda et al., 2020), mouse anti-ZO-1 mAb (Itoh et al., 1991), rabbit anti-occludin pAb (Saitou et al., 1997), rat anti-angulin-1 mAb (Iwamoto et al., 2014), rabbit anti-tricellulin pAb (Oda et al., 2014), rat- α -catenin mAb (clone α 18; Nagafuchi and Tsukita, 1994), rabbit anti-JAM-A pAb (Rehder et al., 2006), rabbit anti-claudin-2 pAb (Kubota et al., 1999), and rabbit anti-claudin-15 pAb (Kiuchi-Saishin et al., 2002) were generated as described previously. Mouse anti-claudin-2 mAb (32-5600), mouse anti-claudin-4 mAb (32-9400), rabbit anti-tricellulin pAb (48-8400), rabbit anti-ZO-2 pAb (38-9100), and rabbit anti-ZO-3 pAb (36-4100) were purchased from Thermo Fisher Scientific. Rat anti-E-cadherin mAb (ECCD-2, M108; Takara Bio), mouse anti- α -tubulin mAb (14-4502-82; eBioscience), rabbit anti- α -catenin pAb (C2081; Sigma-Aldrich), rabbit anti-l/s-afadin pAb (AO224; Sigma-Aldrich), rabbit anti-GFP pAb (598; MBL International), goat anti-aquaporin 2 (AQP2) pAb (C-17; Santa Cruz Biotechnology), and goat anti-GST pAb conjugated with HRP (RPN1236; Amersham Biosciences) were obtained commercially. Alexa Fluor 488-conjugated donkey anti-rabbit, anti-mouse, or anti-rat IgG and Alexa Fluor 647-conjugated donkey anti-goat IgG were obtained from Thermo Fisher Scientific. Cyanine 3-conjugated donkey anti-rabbit, anti-mouse, or anti-rat IgG was purchased from Jackson ImmunoResearch Laboratories. HRP-linked anti-rabbit, anti-mouse, or anti-rat IgG was purchased from GE Healthcare.

Expression vectors and transfection

The cDNA encoding mouse angulin-1 of 575 amino acids was described previously (Higashi et al., 2013). To construct expression vectors for full-length angulin-1 and angulin-1 Δ p_{bm}, cDNAs encoding mouse angulin-1 and its mutant lacking the C-terminal five amino acids were amplified by PCR using

KOD-Plus-Ver.2 DNA polymerase (Toyobo) and subcloned into pCAGGSneodeIcoRI (Niwa et al., 1991). To construct expression vectors for GST fusion of aa 409–575 and aa 409–570 of mouse angulin-1, the corresponding cDNAs of mouse angulin-1 were amplified by PCR using KOD-Plus-Ver.2 DNA polymerase and subcloned into pGEX-6P-1 (GE Healthcare). To construct an expression vector for MBP-tagged N-ZO-1 (aa 1–862), cDNA encoding aa 1–862 of mouse ZO-1 was amplified by PCR using KOD-Plus-Ver.2 DNA polymerase from pCANw-ZO-1-GFP (Otani et al., 2019) and subcloned into pMAL-cRI (New England Biolabs). Expression vectors for MBP fusion proteins of the PDZ1, PDZ2, and PDZ3 domains of ZO-1 (Itoh et al., 2001) were kindly provided by Dr. Masahiko Itoh (Dokkyo Medical University, Tochigi, Japan). To construct an expression vector for a fusion protein of angulin-1Δpbm with ZO-1 (angulin-1Δpbm-ZO-1), the BglII sites within the angulin-1Δpbm cDNA and ZO-1 cDNA were disrupted in advance without changing amino acid sequences by inverse PCR. The cDNA encoding angulin-1Δpbm was amplified by PCR using KOD-Plus-Ver.2 DNA polymerase and subcloned into pCAGGSneodeIcoRI between the NotI site and the BglII site. Next, cDNA encoding ZO-1, in which the BglII site was disrupted, was amplified by PCR using KOD-Plus-Ver.2 DNA polymerase, and the DNA fragments were subcloned into pCAGGSneodeIcoRI between the BglII site and the EcoRI site. To construct an expression vector for a fusion protein of angulin-1Δpbm with the PDZ1 domain of ZO-1 (aa 1–120), the cDNA encoding the fusion protein was amplified by PCR using KOD-Plus-Ver.2 DNA polymerase from an expression vector for angulin-1Δpbm-ZO-1 and digested with BglII and EcoRI to get cDNA fragments encoding the PDZ1 domain of ZO-1. The cDNA fragments were subcloned into an expression vector of angulin-1Δpbm-ZO-1, which was digested with BglII and EcoRI. An expression vector for GFP-tagged ZO-1 lacking the PDZ2 domain (aa 181–292) was constructed by inverse PCR from pCANw-ZO-1-GFP and introduced into ZO-1/ZO-2-dKO cells (Otani et al., 2019).

DNA transfection was performed using the Lipofectamine LTX and Plus Reagent (Thermo Fisher Scientific) according to the manufacturer's instructions. Stable cell lines were selected by treatment with 500 μg/ml G-418 (Nacalai Tesque).

Genome editing

Angulin-1-KO cells were established from parental MDCK II cells by genome editing using TALEN. TALENs were constructed according to the instruction provided by the TALE Toolbox kit from the Zhang laboratory (Sanjana et al., 2012; Addgene; 1000000019). The target sequences for the left arm, spacer, and right arm are indicated in Fig. S1. The construction of the TALEN expression vectors and transfection was performed as described previously (Tokuda et al., 2014). Transfected cell colonies were propagated and screened for angulin-1 depletion by immunofluorescence staining. Angulin-1-KO cell clones were isolated by limiting the dilution of cell colonies containing angulin-1-negative cells. To confirm mutations in the targeting sites in the angulin-1 gene in angulin-1-KO cells, the genomic DNA containing the targeting site was amplified by PCR using a primer set, 5'-GCCCTTTAA CGTCTGGGAC-3' (forward) and 5'-GAGCAACTCTCTACTCCG-3' (reverse), subcloned into pTAC-1 vector (BioDynamics Laboratory Inc.) by TA cloning, and subjected to Sanger sequencing.

Tricellulin-KO cells and claudin/angulin-1-KO cells were generated from parental MDCK II cells and claudin-quinKO cells (Otani et al., 2019), respectively, with Cas9-gRNA RNP complexes using a CUY21 Pro-Vitro electroporator (Nepa Gene). CRISPR RNA for the target sequence, 5'-CGGCATGACCACCTA CTACCGGG-3' for tricellulin or 5'-GGCTGGGGCGGGTCTGTC TTCCGG-3' for angulin-1 (protospacer adjacent motif [PAM] site is underlined), and trans-activating CRISPR RNA were synthesized by Integrated DNA Technologies and annealed with each other. Cas9 proteins (Integrated DNA Technologies) were incubated with the gRNA duplex at RT for 10 min to form Cas9-gRNA RNP complexes (1:1.2 molar ratio). 100 pmol Cas9 and 120 pmol gRNA duplex were introduced into 1×10^6 cells. Electroporation was performed with the following conditions: 150 V for 10 ms (prepulse) and 10 pulses of 20 V for 50 ms at 50-ms intervals (postpulses). Angulin-1/claudin-2-dKO cells and tricellulin/claudin-2-dKO cells were established from claudin-2-KO cells (Tokuda and Furuse, 2015) by CRISPR/Cas9-mediated genome editing of the angulin-1 gene and the tricellulin gene, respectively, using pSpCas9(BB)-2A-Puro(PX459) V2.0 vector (62988; Addgene). The following DNA sense and antisense strands of the targeting sites were annealed with each other in KOD FX Neo buffer (Toyobo): angulin-1, 5'-CACCGGCTGGGGCGGGT CGTCTT-3' (sense) and 5'-AAACAAGACGACCGCGCCAGCC-3' (antisense); tricellulin, 5'-CACCGCGCATGACCACCTACTACC-3' (sense) and 5'-AAACGGTAGTAGGTGGTCATGCCGC-3' (antisense). The obtained DNA duplexes were ligated to pSpCas9(BB)-2A-Puro(PX459) V2.0 digested by BpiI (FD1014; Thermo Fisher Scientific). Claudin-2-KO cells were transfected with the CRISPR/Cas9 vectors using Lipofectamine LTX and Plus Reagent (Thermo Fisher Scientific). The transfected cells were cloned in a glass-bottomed 96-well plate (Corning) by limiting dilution, and the KO cells were selected by immunofluorescence microscopy. To confirm mutations in the corresponding targeting sites, the genomic regions of targeting sequences were amplified by PCR with primer sets of SalI site-containing forward primers and EcoRI site-containing reverse primers. The PCR products were digested with SalI/EcoRI and subcloned into SalI/EcoRI-digested pBluescript SK(-). Mutations in targeting sites were confirmed by Sanger sequencing. The following primers were used for genomic PCR: angulin-1, 5'-GGGGTTCGACCGG AGCGGAGGCGGGAAGGGGAGG-3' (forward) and 5'-GGGGAA TTCCGGCGGTGGGGACTCCATCCATCG-3' (reverse); tricellulin, 5'-GGGGTTCGACGAGCAGCGAGCGGGAGGAGGACTTGC-3' (forward) and 5'-GGGGAATTCACCTCGTGCCTCCACAGCTTCA GG-3' (reverse).

Immunofluorescence microscopy

For immunofluorescence microscopy of cultured cells, cells were seeded at a density of 1.0×10^5 cells/cm² on 12-mm-diameter Transwell filters with 0.4-μm pore size (3401; Corning). After 3–4 d of culture on Transwell filters, cells were fixed with 1% formaldehyde in PBS containing 0.5 mM CaCl₂ for 10 min at RT and washed with PBS three times. The cells were permeabilized with 0.2% Triton X-100 in PBS for 10 min at RT and washed with PBS three times. For immunofluorescence microscopy of frozen sections of mouse tissues, the dissected tissue blocks were

embedded in optimal cutting temperature compound (Sakura Finetek Japan), quickly frozen in liquid nitrogen, and cut into ~6- μm -thick sections with a cryostat at -20°C . The sections were mounted on coverslips, air dried for 30 min, fixed in 95% ethanol on ice for 30 min, and treated with 100% acetone at RT for 1 min followed by washing with PBS three times. All of the cells and mouse tissues were blocked with 1% BSA in PBS for 30 min at RT. The samples were incubated with primary antibodies followed by fluorescence-labeled secondary antibodies. After washing with PBS, the samples were embedded in FluoroSave reagent (EMD Millipore) and observed with a laser scanning confocal microscope (TCS-SPE; Leica Microsystems) equipped with an HCX plan apochromat 63 \times /1.40 NA objective. Images were processed using Fiji/ImageJ software (National Institutes of Health).

Quantification of extended distribution of TJ or tTJ proteins along the apicobasal axis at TCs was done using a binary classification rather than analyzing junction length, because lower resolution along the z axis in confocal microscopy hampers the measurement of true junction length. Confocal sections along the z axis were obtained from each cell line. For each TC, the section of 1.2 μm basal from the section that contained the strongest signal of TJ markers was selected. Then, fluorescence signals of TJ or tTJ proteins at the TC and those at a close bicellular junction were measured by line scan. When the maximum signal at the TC was more than fourfold higher than that at the bicellular junction, we considered that the TJ or tTJ proteins showed extended distribution along the apicobasal axis at the TC. By these measurements throughout a field of view, the ratio of TCs with extended distribution of the TJ or tTJ proteins was calculated. The data from three fields of view were analyzed. To quantify TCs with angulin-1-positive rods colocalizing with ZO-1 in tricellulin-KO cells, the same measurements were performed for fluorescence signals of angulin-1 or ZO-1, except that the confocal section of 1.7 μm basal from the section that contained TJ markers was analyzed. Among TCs with extended distribution of angulin-1, the ratio of TCs with extended distribution of ZO-1 was calculated. Image processing was performed using Fiji/ImageJ software.

EM

For ultrathin section EM of cultured cells, samples were prepared in principle as described previously (Otani et al., 2019). Cells were seeded at a density of 1.0×10^5 cells/ cm^2 on 12-mm-diameter Transwell polycarbonate filters (3401; Corning). After 3–4 d of culture, the cells were fixed with a fixative containing 2% glutaraldehyde, 2% PFA, 20 mM CaCl_2 , and 0.1 M cacodylate buffer, pH 7.4, for 1 h at RT and washed with 0.1 M cacodylate buffer, pH 7.4. Filters were excised by scalpels and postfixed with 1% OsO_4 in 0.1 M cacodylate buffer, pH 7.4, for 1 h on ice. After being washed with water, the samples were stained with 0.5% uranyl acetate for 2 h at RT. After being washed with water, the samples were dehydrated in a graded series of ethanol. The samples were then soaked in propylene oxide for 1–2 min, transferred to a 1:1 mixture of propylene oxide and Quetol 812 resin, and incubated overnight. The samples were embedded in Epon 812 resin. Ultrathin sections of ~60-nm thickness were

collected on copper grids; stained with 0.5% uranyl acetate for 3 min; and then stained with Sato's lead solution containing 1% lead citrate, 1% lead nitrate, and 2% sodium citrate (Sato, 1968) for 3 min. The sections were washed with water and dried. To evaluate whether TCs are closed or open with obvious gaps, we picked the EM images in which lipid bilayers of all of the three plasma membranes at the center of TCs were recognized among the acquired EM images of the TJ or AJC levels. Then, we drew a circle with a 15-nm diameter on the EM images in Photoshop software (Adobe). If the circle did not overlap with a light intermediate layer of any of the three plasma membranes, we judged that the TC was open. Otherwise, we judged that the TC was closed even if we recognized a very narrow space surrounded by the three plasma membranes.

For freeze-fracture EM, cells were seeded at a density of 1.0×10^5 cells/ cm^2 on 24-mm-diameter Transwell polycarbonate filters (3412; Corning). After 3–4 d of culture, the cells were fixed with 2% glutaraldehyde in 0.1 M phosphate buffer, pH 7.4, for 1 h and washed three times with 0.1 M phosphate buffer, pH 7.4. The samples were immersed in 30% glycerol in 0.1 M phosphate buffer, pH 7.4, for 30 min at RT and then frozen with liquid nitrogen. The frozen samples were fractured at -100°C and platinum shadowed unidirectionally at an angle of 45° using a Balzers freeze etching system (BAF060; Bal-Tec). The fractured samples were collected on formvar-filmed grids. Samples were observed with a transmission electron microscope (JEM-1011 or JEM-1010; JEOL) at an accelerating voltage of 80 kV. To evaluate disorganization of the tTJ ultrastructure in tricellulin-KO cells by freeze-fracture EM, we counted the number of short TJ strands connected to a central sealing element in freeze-fracture replicas.

Western blotting and GST pull-down assay

For Western blotting of cell lysates, cells were lysed with Laemmli SDS sample buffer supplemented with 100 mM DTT and boiled at 100°C for 5 min. The proteins were separated by SDS-PAGE using a 10%, 12.5%, or 15% polyacrylamide gel and transferred to polyvinylidene fluoride membrane with 0.45- μm pore size (EMD Millipore). The membranes were blocked with 5% skim milk in TBS supplemented with 0.1% Tween 20 (TBS-T) and incubated with primary antibodies diluted with 5% skim milk in TBS-T or immunoreaction enhancer solution of Can Get Signal (NKB-101; Toyobo) for 1 h at 37°C . After the incubation, the membranes were washed three times with TBS-T, followed by incubation of HRP-linked secondary antibodies diluted with 5% skim milk in TBS-T or immunoreaction enhancer solution of Can Get Signal (NKB-101; Toyobo) for 1 h at 37°C . After the incubation, the membranes were rinsed three times with TBS-T. The secondary antibodies were detected by ECL (ECL Prime; GE Healthcare). Images were obtained with a LAS3000 Mini imager (Fujifilm) and processed using Fiji/ImageJ software (National Institutes of Health).

For in vitro binding assays, all of the GST-tagged or MBP-tagged proteins were expressed in *Escherichia coli* (DH5 α). For GST pull-down assays using lysates of angulin-1-KO cells, angulin-1-KO cells were lysed with the lysis buffer (0.5% NP-40, 50 mM Tris-HCl, pH 7.4, 150 mM NaCl, 2 mM EDTA, 10%

glycerol) supplemented with 1 mM DTT and protease inhibitor cocktail (Nacalai Tesque). After centrifugation of the lysates, the supernatant fluids were incubated with glutathione sepharose 4B beads coupled with GST or GST-angulin-1 cytoplasmic region (aa 409–575) for 2–3 h at 4°C. The beads were washed three times with lysis buffer and boiled with 2× Laemmli SDS sample buffer supplemented with 100 mM DTT. For in vitro binding assays between angulin-1 and ZO-1, MBP-tagged proteins of ZO-1 (N-ZO-1, 1–862 aa; PDZ1 domain, 19–113 aa; PDZ2 domain, 181–292 aa; or PDZ3 domain, 423–503 aa) were incubated with GST or GST-tagged angulin-1 cytoplasmic region (409–575 aa or 409–570 aa) for 2–3 h at 4°C and further incubated with glutathione sepharose 4B beads (GE Healthcare) for 1 h at 4°C. The beads were washed three times with lysis buffer and boiled with 2× Laemmli SDS sample buffer supplemented with 100 mM DTT. The lysates were analyzed by SDS-PAGE and Western blotting.

TER and paracellular tracer flux

MDCK II cells were seeded at a density of 1.0×10^5 cells/cm² on 12-mm-diameter Transwell polycarbonate filters with 0.4- μ m pore size (3401; Corning) and cultured for 4–5 d. Electrical resistance was measured using Millicell ERS-2 (EMD Millipore). Electrical resistance of Transwell filters without cells was measured as a blank. The mean blank value was subtracted from electrical resistance, and TER was determined by multiplying the electrical resistance by the growth area of the Transwell filter. To measure paracellular tracer flux, medium was changed to phenol-red free DMEM (08489-45; Nacalai Tesque) supplemented with 10% FBS and 2 mM L-glutamine (16948-04; Nacalai Tesque). On the following day, 200 μ M fluorescein (16106-82; Nacalai Tesque) or 50 μ M 150 kD FITC-dextran (FD150S; Sigma-Aldrich) was added to the apical chamber. Medium volumes of the apical and basal chambers were 250 μ l and 1 ml, respectively. The cells were incubated for 2 h at 37°C and 5% CO₂. The medium of the basal chamber was collected, and the fluorescence intensity of the medium was measured by a microplate reader (SpectraMax Paradigm; Molecular Devices). Fluorescence intensity of medium without fluorescent tracer was measured as a blank. After subtraction of the mean blank values from fluorescence intensities of the samples, the apparent permeability (P_{app}) was calculated using the following equation: $P_{app} = (dQ/dt)/A C_0$ (dQ is the amount of tracer transported to the basal chamber, dt is incubation time, A is the area of the Transwell filters, and C₀ is the initial concentration of tracer in the apical chamber).

Online supplemental material

Fig. S1 shows the localization of TJ and tTJ proteins in the proximal tubules and MDCK II cells. Fig. S2 shows characterization of angulin-1-KO cells, those expressing exogenous angulin-1 constructs, claudin-quinKO cells, claudin/JAM-A-KO cells, and JAM-A-KO cells. Fig. S3 shows characterization of angulin-1/claudin-2-dKO cells and those expressing exogenous angulin-1 constructs in terms of the epithelial barrier function. Fig. S4 shows the behavior of angulin-1 in ZO-1/ZO-1-dKO cells and those expressing exogenous full-length ZO-1 or a ZO-1

mutant lacking the PDZ2 domain. Fig. S5 shows characterization of tricellulin-KO cells and tricellulin/claudin-2-dKO cells in terms of the epithelial barrier function and tTJ morphology.

Acknowledgments

We thank Shinsaku Tokuda for designing TALEN constructs; Akira Nagafuchi (Nara Medical University, Nara, Japan), Klaus Ebnet (University of Münster, Münster, Germany), Masayuki Murata (University of Tokyo, Tokyo, Japan), and Masahiko Itoh (Dokkyo Medical University, Tochigi, Japan) for kindly providing reagents; the EM facility in the National Institute for Physiological Sciences for support in EM; Osamu Nagata, Mika Watanabe, and Yuichiro Kano for technical assistance; Motohiro Nishida for use of a microplate reader; and Akira Nagafuchi, Shigenobu Yonemura, and all members of the Furuse laboratory for discussions. We also thank Alison Sherwin, PhD, from Edanz Group (<https://en-author-services.edanzgroup.com/>) for editing a draft of the manuscript.

This work was supported by a Japan Society for the Promotion of Science Grant-in-Aid for Challenging Exploratory Research (16K15226), Japan Society for the Promotion of Science Grants-in-Aid for Scientific Research (B; 26291043, 18H02440, and 21H02523), and a Life Science Aid grant from the Takeda Science Foundation to M. Furuse.

The authors declare no competing financial interests.

Author contributions: T. Sugawara and M. Furuse designed the study. T. Sugawara performed most of the experiments except EM and data analysis. T. Otani contributed to key materials. K. Furuse performed most of the EM analyses of ultrathin sections and freeze-fracture replicas. T. Wakayama performed quantification of TJ strands in freeze-fracture replicas. T. Sugawara and M. Furuse wrote the manuscript. All authors read and commented on the manuscript.

Submitted: 22 May 2020

Revised: 24 April 2021

Accepted: 21 June 2021

References

- Amasheh, S., N. Meiri, A.H. Gitter, T. Schöneberg, J. Mankertz, J.D. Schulzke, and M. Fromm. 2002. Claudin-2 expression induces cation-selective channels in tight junctions of epithelial cells. *J. Cell Sci.* 115:4969–4976. <https://doi.org/10.1242/jcs.00165>
- Belardi, B., S. Son, M.D. Vahey, J. Wang, J. Hou, and D.A. Fletcher. 2018. Claudin-4 reconstituted in unilamellar vesicles is sufficient to form tight interfaces that partition membrane proteins. *J. Cell Sci.* 132: jcs221556. <https://doi.org/10.1242/jcs.221556>
- Borck, G., A. Ur Rehman, K. Lee, H.M. Pogoda, N. Kakar, S. von Ameln, N. Grillet, M.S. Hildebrand, Z.M. Ahmed, G. Nürnberg, et al. 2011. Loss-of-function mutations of ILDR1 cause autosomal-recessive hearing impairment DFNB42. *Am. J. Hum. Genet.* 88:127–137. <https://doi.org/10.1016/j.ajhg.2010.12.011>
- Byri, S., T. Misra, Z.A. Syed, T. Bätz, J. Shah, L. Boril, J. Glashauser, T. Aegerter-Wilmsen, T. Matzat, B. Moussian, et al. 2015. The triple-repeat protein Anakonda controls epithelial tricellular junction formation in *Drosophila*. *Dev. Cell.* 33:535–548. <https://doi.org/10.1016/j.devcel.2015.03.023>
- Cavey, M., and T. Lecuit. 2009. Molecular bases of cell-cell junctions stability and dynamics. *Cold Spring Harb. Perspect. Biol.* 1:a002998. <https://doi.org/10.1101/cshperspect.a002998>

- Cerejido, M., E.S. Robbins, W.J. Dolan, C.A. Rotunno, and D.D. Sabatini. 1978. Polarized monolayers formed by epithelial cells on a permeable and translucent support. *J. Cell Biol.* 77:853–880. <https://doi.org/10.1083/jcb.77.3.853>
- Claude, P., and D.A. Goodenough. 1973. Fracture faces of zonulae occludentes from “tight” and “leaky” epithelia. *J. Cell Biol.* 58:390–400. <https://doi.org/10.1083/jcb.58.2.390>
- Cording, J., J. Berg, N. Käding, C. Bellmann, C. Tscheik, J.K. Westphal, S. Milatz, D. Günzel, H. Wolburg, J. Piontek, et al. 2013. In tight junctions, claudins regulate the interactions between occludin, tricellulin and marvelD3, which, inversely, modulate claudin oligomerization. *J. Cell Sci.* 126:554–564. <https://doi.org/10.1242/jcs.114306>
- Dunn, B.S., L. Rush, J.Y. Lu, and T. Xu. 2018. Mutations in the *Drosophila* tricellular junction protein M6 synergize with Ras^{V12} to induce apical cell delamination and invasion. *Proc. Natl. Acad. Sci. USA.* 115:8358–8363. <https://doi.org/10.1073/pnas.1807343115>
- Esmangart de Bournonville, T., and R. Le Borgne. 2020. Interplay between Anakonda, Gliotactin, and M6 for tricellular junction assembly and anchoring of septate junctions in *Drosophila* epithelium. *Curr. Biol.* 30:4245–4253.e4. <https://doi.org/10.1016/j.cub.2020.07.090>
- Fanning, A.S., B.J. Jameson, L.A. Jesaitis, and J.M. Anderson. 1998. The tight junction protein ZO-1 establishes a link between the transmembrane protein occludin and the actin cytoskeleton. *J. Biol. Chem.* 273:29745–29753. <https://doi.org/10.1074/jbc.273.45.29745>
- Farquhar, M.G., and G.E. Palade. 1963. Junctional complexes in various epithelia. *J. Cell Biol.* 17:375–412. <https://doi.org/10.1083/jcb.17.2.375>
- Finegan, T.M., N. Hervieux, A. Nestor-Bergmann, A.G. Fletcher, G.B. Blanchard, and B. Sanson. 2019. The tricellular vertex-specific adhesion molecule Sidekick facilitates polarised cell intercalation during *Drosophila* axis extension. *PLoS Biol.* 17:e3000522. <https://doi.org/10.1371/journal.pbio.3000522>
- Furuse, M., H. Sasaki, and S. Tsukita. 1999. Manner of interaction of heterogeneous claudin species within and between tight junction strands. *J. Cell Biol.* 147:891–903. <https://doi.org/10.1083/jcb.147.4.891>
- Furuse, M., K. Furuse, H. Sasaki, and S. Tsukita. 2001. Conversion of zonulae occludentes from tight to leaky strand type by introducing claudin-2 into Madin-Darby canine kidney I cells. *J. Cell Biol.* 153:263–272. <https://doi.org/10.1083/jcb.153.2.263>
- Furuse, M., Y. Izumi, Y. Oda, T. Higashi, and N. Iwamoto. 2014. Molecular organization of tricellular tight junctions. *Tissue Barriers.* 2:e28960. <https://doi.org/10.1016/j.tisb.28960>
- Gong, Y., N. Himmerkus, A. Sunq, S. Milatz, C. Merkel, M. Bleich, and J. Hou. 2017. ILDR1 is important for paracellular water transport and urine concentration mechanism. *Proc. Natl. Acad. Sci. USA.* 114:5271–5276. <https://doi.org/10.1073/pnas.1701006114>
- Hempstock, W., S. Sugioka, N. Ishizuka, T. Sugawara, M. Furuse, and H. Hayashi. 2020. Angulin-2/ILDR1, a tricellular tight junction protein, does not affect water transport in the mouse large intestine. *Sci. Rep.* 10:10374. <https://doi.org/10.1038/s41598-020-67319-5>
- Higashi, T., S. Tokuda, S. Kitajiri, S. Masuda, H. Nakamura, Y. Oda, and M. Furuse. 2013. Analysis of the ‘angulin’ proteins LSR, ILDR1 and ILDR2—tricellulin recruitment, epithelial barrier function and implication in deafness pathogenesis. *J. Cell Sci.* 126:966–977. <https://doi.org/10.1242/jcs.138271>
- Higashi, T., T. Katsuno, S. Kitajiri, and M. Furuse. 2015. Deficiency of angulin-2/ILDR1, a tricellular tight junction-associated membrane protein, causes deafness with cochlear hair cell degeneration in mice. *PLoS One.* 10:e0120674. <https://doi.org/10.1371/journal.pone.0120674>
- Honda, H. 1983. Geometrical Models for Cells in Tissues. In *International Review of Cytology*. Elsevier. pp. 191–248.
- Ikenouchi, J., M. Furuse, K. Furuse, H. Sasaki, S. Tsukita, and S. Tsukita. 2005. Tricellulin constitutes a novel barrier at tricellular contacts of epithelial cells. *J. Cell Biol.* 171:939–945. <https://doi.org/10.1083/jcb.200510043>
- Ikenouchi, J., H. Sasaki, S. Tsukita, M. Furuse, and S. Tsukita. 2008. Loss of occludin affects tricellular localization of tricellulin. *Mol. Biol. Cell.* 19:4687–4693. <https://doi.org/10.1091/mbc.e08-05-0530>
- Itoh, M., S. Yonemura, A. Nagafuchi, S. Tsukita, and S. Tsukita. 1991. A 220-kD undercoat-constitutive protein: its specific localization at cadherin-based cell-cell adhesion sites. *J. Cell Biol.* 115:1449–1462. <https://doi.org/10.1083/jcb.115.5.1449>
- Itoh, M., A. Nagafuchi, S. Yonemura, T. Kitani-Yasuda, S. Tsukita, and S. Tsukita. 1993. The 220-kD protein colocalizing with cadherins in non-epithelial cells is identical to ZO-1, a tight junction-associated protein in epithelial cells: cDNA cloning and immunoelectron microscopy. *J. Cell Biol.* 121:491–502. <https://doi.org/10.1083/jcb.121.3.491>
- Itoh, M., M. Furuse, K. Morita, K. Kubota, M. Saitou, and S. Tsukita. 1999. Direct binding of three tight junction-associated MAGUKs, ZO-1, ZO-2, and ZO-3, with the COOH termini of claudins. *J. Cell Biol.* 147:1351–1363. <https://doi.org/10.1083/jcb.147.6.1351>
- Itoh, M., H. Sasaki, M. Furuse, H. Ozaki, T. Kita, and S. Tsukita. 2001. Junctional adhesion molecule (JAM) binds to PAR-3: a possible mechanism for the recruitment of PAR-3 to tight junctions. *J. Cell Biol.* 154:491–498. <https://doi.org/10.1083/jcb.200103047>
- Iwamoto, N., T. Higashi, and M. Furuse. 2014. Localization of angulin-1/LSR and tricellulin at tricellular contacts of brain and retinal endothelial cells in vivo. *Cell Struct. Funct.* 39:1–8. <https://doi.org/10.1247/csf.13015>
- Kamitani, T., H. Sakaguchi, A. Tamura, T. Miyashita, Y. Yamazaki, R. Tokumasu, R. Inamoto, A. Matsubara, N. Mori, Y. Hisa, et al. 2015. Deletion of tricellulin causes progressive hearing loss associated with degeneration of cochlear hair cells. *Sci. Rep.* 5:18402. <https://doi.org/10.1038/srep18402>
- Kiuchi-Saishin, Y., S. Gotoh, M. Furuse, A. Takasuga, Y. Tano, and S. Tsukita. 2002. Differential expression patterns of claudins, tight junction membrane proteins, in mouse nephron segments. *J. Am. Soc. Nephrol.* 13:875–886. <https://doi.org/10.1681/ASN.V134875>
- Krug, S.M., S. Amasheh, J.F. Richter, S. Milatz, D. Günzel, J.K. Westphal, O. Huber, J.D. Schulzke, and M. Fromm. 2009. Tricellulin forms a barrier to macromolecules in tricellular tight junctions without affecting ion permeability. *Mol. Biol. Cell.* 20:3713–3724. <https://doi.org/10.1091/mbc.e09-01-0080>
- Kubota, K., M. Furuse, H. Sasaki, N. Sonoda, K. Fujita, A. Nagafuchi, and S. Tsukita. 1999. Ca²⁺-independent cell-adhesion activity of claudins, a family of integral membrane proteins localized at tight junctions. *Curr. Biol.* 9(18):1035–S1. [https://doi.org/10.1016/s0960-9822\(99\)80452-7](https://doi.org/10.1016/s0960-9822(99)80452-7)
- Letizia, A., D. He, S. Astigarraga, J. Colombelli, V. Hatini, M. Llimargas, and J.E. Treisman. 2019. Sidekick is a key component of tricellular adherens junctions that acts to resolve cell rearrangements. *Dev. Cell.* 50:313–326.e5. <https://doi.org/10.1016/j.devcel.2019.07.007>
- Maddirevula, S., H. Alhebbi, A. Alqahtani, T. Algoufi, H.S. Alsaif, N. Ibrahim, F. Abdulwahab, M. Barr, H. Alzaidan, A. Almehaideb, et al. 2019. Identification of novel loci for pediatric cholestatic liver disease defined by KIF12, PPM1F, USP53, LSR, and WDR83OS pathogenic variants. *Genet. Med.* 21:1164–1172. <https://doi.org/10.1038/s41436-018-0288-x>
- Masuda, S., Y. Oda, H. Sasaki, J. Ikenouchi, T. Higashi, M. Akashi, E. Nishi, and M. Furuse. 2011. LSR defines cell corners for tricellular tight junction formation in epithelial cells. *J. Cell Sci.* 124:548–555. <https://doi.org/10.1242/jcs.072058>
- Mesli, S., S. Javorschi, A.M. Bérard, M. Landry, H. Priddle, D. Kivlichan, A.J.H. Smith, F.T. Yen, B.E. Bihain, and M. Darmon. 2004. Distribution of the lipolysis stimulated receptor in adult and embryonic murine tissues and lethality of LSR^{-/-} embryos at 12.5 to 14.5 days of gestation. *Eur. J. Biochem.* 271:3103–3114. <https://doi.org/10.1111/j.1432-1033.2004.04223.x>
- Morozko, E.L., A. Nishio, N.J. Ingham, R. Chandra, T. Fitzgerald, E. Martelletti, G. Borck, E. Wilson, G.P. Riordan, P. Wangemann, et al. 2015. ILDR1 null mice, a model of human deafness DFNB42, show structural aberrations of tricellular tight junctions and degeneration of auditory hair cells. *Hum. Mol. Genet.* 24:609–624. <https://doi.org/10.1093/hmg/ddu474>
- Nagafuchi, A., and S. Tsukita. 1994. The loss of the expression of a catenin, the 102 kD cadherin associated protein, in central nervous tissues during development: α catenin/cadherin/cell adhesion/CNS. *Dev. Growth Differ.* 36:59–71. <https://doi.org/10.1111/j.1440-169X.1994.00059.x>
- Nayak, G., S.I. Lee, R. Yousaf, S.E. Edelmann, C. Trincot, C.M. Van Itallie, G.P. Sinha, M. Rafeeq, S.M. Jones, I.A. Belyantseva, et al. 2013. Tricellulin deficiency affects tight junction architecture and cochlear hair cells. *J. Clin. Invest.* 123:4036–4049. <https://doi.org/10.1172/JCI69031>
- Nayak, G., L. Varga, C. Trincot, M. Shahzad, P.L. Friedman, I. Klimes, J.H. Greinwald Jr., S.A. Riazuddin, I. Masindova, M. Profant, et al. 2015. Molecular genetics of MARVELD2 and clinical phenotype in Pakistani and Slovak families segregating DFNB49 hearing loss. *Hum. Genet.* 134:423–437. <https://doi.org/10.1007/s00439-015-1532-y>
- Niwa, H., K. Yamamura, and J. Miyazaki. 1991. Efficient selection for high-expression transfectants with a novel eukaryotic vector. *Gene.* 108:193–199. [https://doi.org/10.1016/0378-1119\(91\)90434-D](https://doi.org/10.1016/0378-1119(91)90434-D)
- Oda, Y., T. Otani, J. Ikenouchi, and M. Furuse. 2014. Tricellulin regulates junctional tension of epithelial cells at tricellular contacts through Cdc42. *J. Cell Sci.* 127:4201–4212. <https://doi.org/10.1242/jcs.150607>
- Oda, Y., T. Sugawara, Y. Fukata, Y. Izumi, T. Otani, T. Higashi, M. Fukata, and M. Furuse. 2020. The extracellular domain of angulin-1 and

- palmitoylation of its cytoplasmic region are required for angulin-1 assembly at tricellular contacts. *J. Biol. Chem.* 295:4289–4302. <https://doi.org/10.1074/jbc.RA119.010491>
- Atani, T., T.P. Nguyen, S. Tokuda, K. Sugihara, T. Sugawara, K. Furuse, T. Miura, K. Ebnet, and M. Furuse. 2019. Claudins and JAM-A coordinately regulate tight junction formation and epithelial polarity. *J. Cell Biol.* 218: 3372–3396. <https://doi.org/10.1083/jcb.201812157>
- Phua, D.C.Y., J. Xu, S.M. Ali, A. Boey, N.V. Gounko, and W. Hunziker. 2014. ZO-1 and ZO-2 are required for extra-embryonic endoderm integrity, primitive ectoderm survival and normal cavitation in embryoid bodies derived from mouse embryonic stem cells. *PLoS One.* 9:e99532. <https://doi.org/10.1371/journal.pone.0099532>
- Rehder, D., S. Iden, I. Nasdala, J. Wegener, M.K.M.Z. Brickwedde, D. Vestweber, and K. Ebnet. 2006. Junctional adhesion molecule-A participates in the formation of apico-basal polarity through different domains. *Exp. Cell Res.* 312:3389–3403. <https://doi.org/10.1016/j.yexcr.2006.07.004>
- Riazuddin, S., Z.M. Ahmed, A.S. Fanning, A. Lagziel, S. Kitajiri, K. Ramzan, S.N. Khan, P. Chattaraj, P.L. Friedman, J.M. Anderson, et al. 2006. Tricellulin is a tight-junction protein necessary for hearing. *Am. J. Hum. Genet.* 79:1040–1051. <https://doi.org/10.1086/510022>
- Saito, A.C., T. Higashi, Y. Fukazawa, T. Otani, M. Tauchi, A.Y. Higashi, M. Furuse, and H. Chiba. 2021. Occludin and tricellulin facilitate formation of anastomosing tight-junction strand network to improve barrier function. *Anat. Biol. Cell.* 32(8):722–738. <https://doi.org/10.1091/mbc.E20-07-0464>
- Saitou, M., Y. Ando-Akatsuka, M. Itoh, M. Furuse, J. Inazawa, K. Fujimoto, and S. Tsukita. 1997. Mammalian occludin in epithelial cells: its expression and subcellular distribution. *Eur. J. Cell Biol.* 73:222–231.
- Sang, Q., W. Li, Y. Xu, R. Qu, Z. Xu, R. Feng, L. Jin, L. He, H. Li, and L. Wang. 2015. ILDR1 deficiency causes degeneration of cochlear outer hair cells and disrupts the structure of the organ of Corti: a mouse model for human DFNB42. *Biol. Open.* 4:411–418. <https://doi.org/10.1242/bio.201410876>
- Sanjana, N.E., L. Cong, Y. Zhou, M.M. Cuniff, G. Feng, and F. Zhang. 2012. A transcription activator-like effector toolbox for genome engineering. *Nat. Protoc.* 7:171–192. <https://doi.org/10.1038/nprot.2011.431>
- Sasaki, H., C. Matsui, K. Furuse, Y. Mimori-Kiyosue, M. Furuse, and S. Tsukita. 2003. Dynamic behavior of paired claudin strands within apposing plasma membranes. *Proc. Natl. Acad. Sci. USA.* 100:3971–3976. <https://doi.org/10.1073/pnas.0630649100>
- Sato, T. 1968. A modified method for lead staining of thin sections. *J. Electron Microsc. (Tokyo).* 17:158–159. <https://doi.org/10.1093/oxfordjournals.jmicro.a049610>
- Schulte, J., U. Tepass, and V.J. Auld. 2003. Gliotactin, a novel marker of tricellular junctions, is necessary for septate junction development in *Drosophila*. *J. Cell Biol.* 161:991–1000. <https://doi.org/10.1083/jcb.200303192>
- Shukla, P., C. Vogl, B. Wallner, D. Rigler, M. Müller, and S. Macho-Maschler. 2015. High-throughput mRNA and miRNA profiling of epithelial-mesenchymal transition in MDCK cells. *BMC Genomics.* 16:944. <https://doi.org/10.1186/s12864-015-2036-9>
- Sohet, F., C. Lin, R.N. Munji, S.Y. Lee, N. Ruderisch, A. Soung, T.D. Arnold, N. Derugin, Z.S. Vexler, F.T. Yen, et al. 2015. LSR/angulin-1 is a tricellular tight junction protein involved in blood-brain barrier formation. *J. Cell Biol.* 208:703–711. <https://doi.org/10.1083/jcb.201410131>
- Sonoda, N., M. Furuse, H. Sasaki, S. Yonemura, J. Katahira, Y. Horiguchi, and S. Tsukita. 1999. *Clostridium perfringens* enterotoxin fragment removes specific claudins from tight junction strands: evidence for direct involvement of claudins in tight junction barrier. *J. Cell Biol.* 147:195–204. <https://doi.org/10.1083/jcb.147.1.195>
- Staehelein, L.A. 1973. Further observations on the fine structure of freeze-cleaved tight junctions. *J. Cell Sci.* 13:763–786. <https://doi.org/10.1242/jcs.13.3.763>
- Staehelein, L.A., T.M. Mukherjee, and A.W. Williams. 1969. Freeze-etch appearance of the tight junctions in the epithelium of small and large intestine of mice. *Protoplasma.* 67:165–184. <https://doi.org/10.1007/BF01248737>
- Stevenson, B.R., J.M. Anderson, D.A. Goodenough, and M.S. Mooseker. 1988. Tight junction structure and ZO-1 content are identical in two strains of Madin-Darby canine kidney cells which differ in transepithelial resistance. *J. Cell Biol.* 107:2401–2408. <https://doi.org/10.1083/jcb.107.6.2401>
- Tokuda, S., and M. Furuse. 2015. Claudin-2 knockout by TALEN-mediated gene targeting in MDCK cells: claudin-2 independently determines the leaky property of tight junctions in MDCK cells. *PLoS One.* 10:e0119869. <https://doi.org/10.1371/journal.pone.0119869>
- Tokuda, S., T. Higashi, and M. Furuse. 2014. ZO-1 knockout by TALEN-mediated gene targeting in MDCK cells: involvement of ZO-1 in the regulation of cytoskeleton and cell shape. *PLoS One.* 9:e104994. <https://doi.org/10.1371/journal.pone.0104994>
- Tsukita, S., M. Furuse, and M. Itoh. 2001. Multifunctional strands in tight junctions. *Nat. Rev. Mol. Cell Biol.* 2:285–293. <https://doi.org/10.1038/35067088>
- Uechi, H., and E. Kuranaga. 2019. The tricellular junction protein Sidekick regulates vertex dynamics to promote bicellular junction extension. *Dev. Cell.* 50:327–338.e5. <https://doi.org/10.1016/j.devcel.2019.06.017>
- Uehara, T., M. Yamada, S. Umetsu, H. Nittono, H. Suzuki, T. Fujisawa, T. Takenouchi, A. Inui, and K. Kosaki. 2020. Biallelic mutations in the LSR gene cause a novel type of infantile intrahepatic cholestasis. *J. Pediatr.* 221:251–254. <https://doi.org/10.1016/j.jpeds.2020.01.064>
- Umeda, K., J. Ikenouchi, S. Katahira-Tayama, K. Furuse, H. Sasaki, M. Nakayama, T. Matsui, S. Tsukita, M. Furuse, and S. Tsukita. 2006. ZO-1 and ZO-2 independently determine where claudins are polymerized in tight-junction strand formation. *Cell.* 126:741–754. <https://doi.org/10.1016/j.cell.2006.06.043>
- Van Itallie, C.M., and J.M. Anderson. 2014. Architecture of tight junctions and principles of molecular composition. *Semin. Cell Dev. Biol.* 36:157–165. <https://doi.org/10.1016/j.semcdb.2014.08.011>
- Van Itallie, C.M., A.J. Tietgens, and J.M. Anderson. 2017. Visualizing the dynamic coupling of claudin strands to the actin cytoskeleton through ZO-1. *Mol. Biol. Cell.* 28:524–534. <https://doi.org/10.1091/mbc.e16-10-0698>
- Wade, J.B., and M.J. Karnovsky. 1974. The structure of the zonula occludens. A single fibril model based on freeze-fracture. *J. Cell Biol.* 60:168–180. <https://doi.org/10.1083/jcb.60.1.168>
- Walker, D.C., A. MacKenzie, W.C. Hulbert, and J.C. Hogg. 1985. A re-assessment of the tricellular region of epithelial cell tight junctions in trachea of guinea pig. *Acta Anat. (Basel).* 122:35–38. <https://doi.org/10.1159/000145982>
- Willott, E., M.S. Balda, A.S. Fanning, B. Jameson, C. Van Itallie, and J.M. Anderson. 1993. The tight junction protein ZO-1 is homologous to the *Drosophila* discs-large tumor suppressor protein of septate junctions. *Proc. Natl. Acad. Sci. USA.* 90:7834–7838. <https://doi.org/10.1073/pnas.90.16.7834>
- Witteck, A., M. Hollmann, R. Schleutker, and S. Luschnig. 2020. The transmembrane proteins M6 and Anakonda cooperate to initiate tricellular junction assembly in epithelia of *Drosophila*. *Curr. Biol.* 30:4254–4262.e5. <https://doi.org/10.1016/j.cub.2020.08.003>
- Yonemura, S., Y. Wada, T. Watanabe, A. Nagafuchi, and M. Shibata. 2010. α -Catenin as a tension transducer that induces adherens junction development. *Nat. Cell Biol.* 12:533–542. <https://doi.org/10.1038/ncb2055>
- Zihni, C., C. Mills, K. Matter, and M.S. Balda. 2016. Tight junctions: from simple barriers to multifunctional molecular gates. *Nat. Rev. Mol. Cell Biol.* 17:564–580. <https://doi.org/10.1038/nrm.2016.80>

Supplemental material

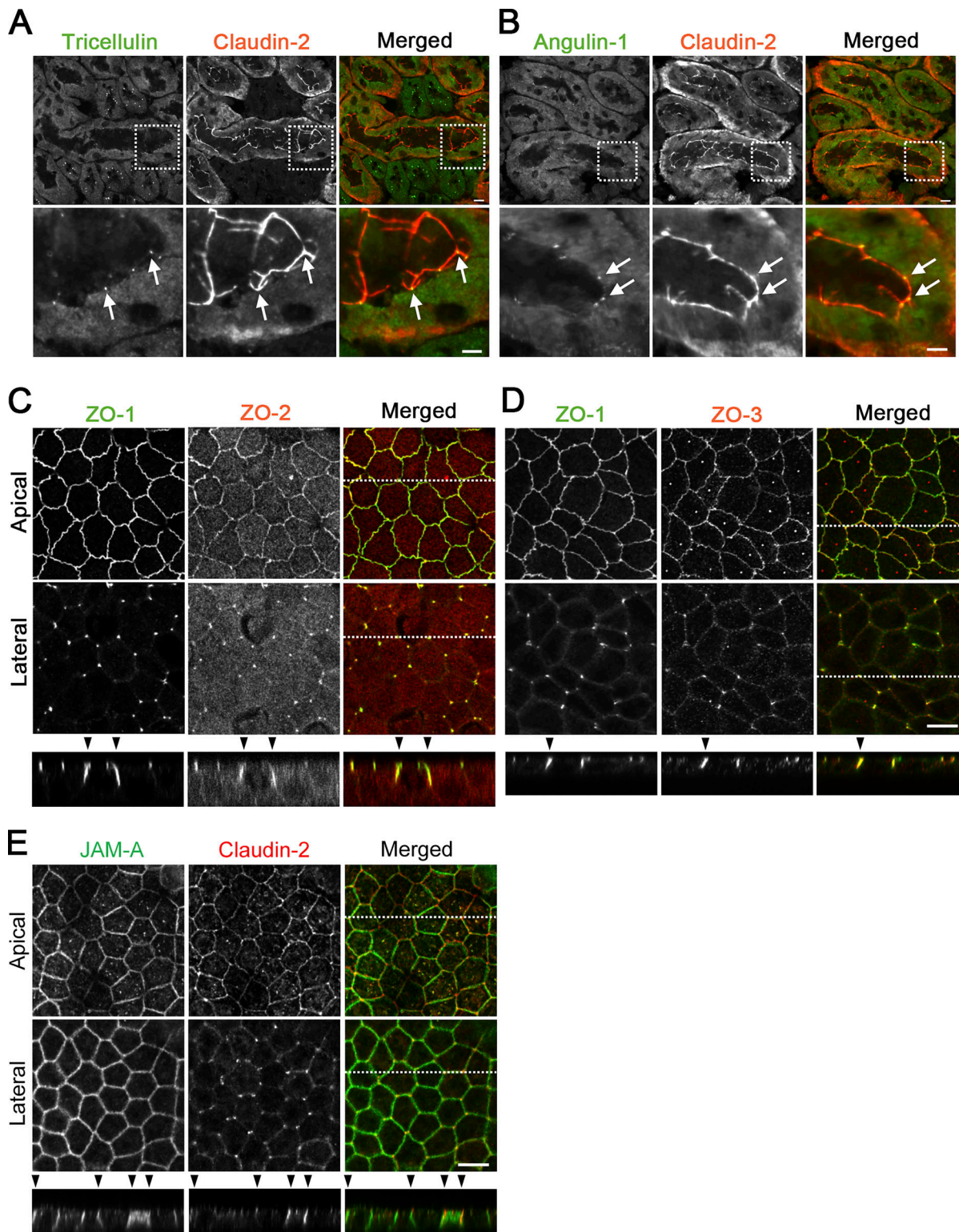


Figure S1. **Localization of TJ and tTJ proteins at TCs.** (A and B) Double-immunofluorescence staining of frozen mouse kidney sections containing proximal tubules with anti-tricellulin mAb and anti-claudin-2 pAb (A) and anti-angulin-1 mAb and anti-claudin-2 pAb (B). Tricellulin and angulin-1 showed dotlike staining at TCs with claudin-2 staining (arrows). (C-E) Double-immunofluorescence staining of MDCK II cells with anti-ZO-1 mAb and anti-ZO-2 pAb (C), anti-ZO-1 mAb and anti-ZO-3 pAb (D), and anti-JAM-A pAb and anti-claudin-2 mAb (E). Confocal sections in the apical region, including TJ markers and the lateral region, together with the corresponding Z-stack images along the white dotted lines are shown. Arrowheads indicate TCs. Bars: 10 μ m (top of A and B and C-E), 5 μ m (bottom of A and B).

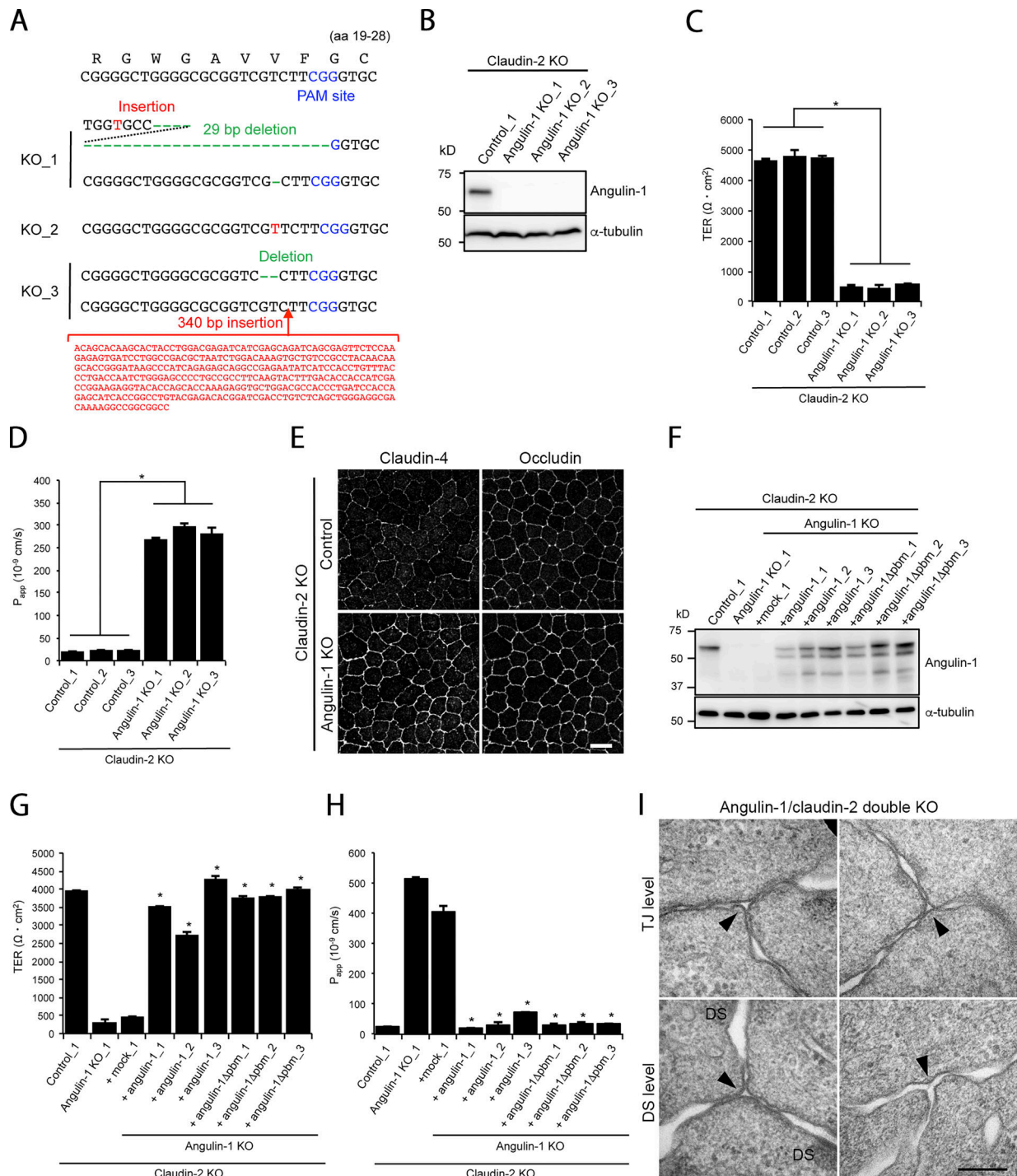


Figure S3. **Characterization of angulin-1/claudin-2-dKO cells and their derivatives.** (A) Frameshift mutations introduced upstream of the PAM site in the angulin-1 gene in angulin-1/claudin-2-dKO cell clones generated by CRISPR/Cas9-mediated genome editing. (B) Western blotting of lysates of a control claudin-2-KO cell clone and three angulin-1/claudin-2-dKO cell clones with anti-angulin-1 pAb or anti-α-tubulin mAb. (C and D) TER (C) and paracellular flux of fluorescein (D) were measured in three control claudin-2-KO cell clones and three angulin-1/claudin-2-dKO cell clones. Data for TER and paracellular flux of fluorescein were analyzed by Student's *t* test and Welch's *t* test, respectively ($n = 9$ total for three control clones [$n = 3$ per clone] versus $n = 9$ total for three angulin-1/claudin-2-dKO clones [$n = 3$ per clone]). P_{app} , apparent permeability. (E) Double-immunofluorescence staining of a control clone of claudin-2-KO cells and an angulin-1/claudin-2-dKO cell clone with anti-claudin-4 mAb and anti-occludin mAb. Bar: 10 μm. (F) Western blotting of lysates of a control claudin-2-KO cell clone, an angulin-1/claudin-2-dKO cell clone, a mock-transfected angulin-1/claudin-2-dKO cell clone, three angulin-1/claudin-2-dKO cell clones expressing exogenous angulin-1, and three angulin-1/claudin-2-dKO cell clones expressing exogenous angulin-1Δpbm with anti-angulin-1 pAb or anti-α-tubulin mAb. (G and H) TER (G) and paracellular flux of fluorescein (H) were measured in the stable cell clones shown in F. Data were analyzed by Dunnett's test ($n = 3$ for the mock cell clone versus $n = 3$ for each angulin-1- or angulin-1Δpbm-expressing clone). Data in C, D, G, and H are shown as mean ± SD ($n = 3$). *, $P < 0.01$. (I) EM observation of horizontal ultrathin sections of an angulin-1/claudin-2-dKO cell clone. Images of TCs at the TJ level and DS level are shown. Apparent gaps are observed (arrowheads). Bar: 200 nm.

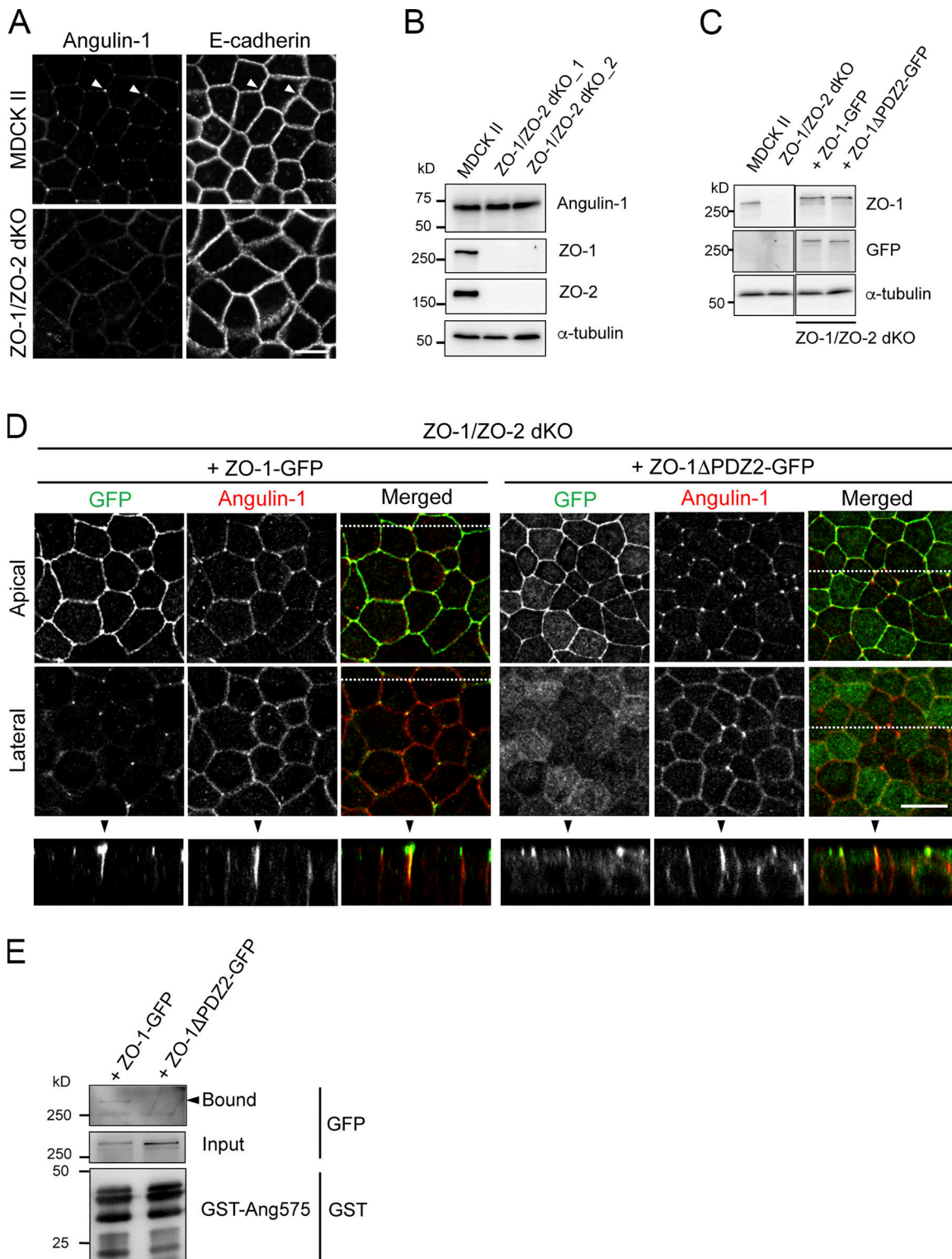


Figure S4. **Characterization of ZO-1/ZO-2-dKO cells expressing ZO-1 and its mutant.** **(A)** Double-immunofluorescence staining of MDCK II cells and ZO-1/ZO-2-dKO cells with anti-angulin-1 pAb and anti-E-cadherin mAb. Arrowheads indicate TCs. Bar: 10 μ m. **(B)** Western blotting of lysates of MDCK II cells and two ZO-1/ZO-2-dKO clones with anti-angulin-1 pAb, anti-ZO-1 mAb, anti-ZO-2 pAb, or anti- α -tubulin mAb. **(C)** Western blotting of lysates of MDCK II cells, ZO-1/ZO-2-dKO cells, and ZO-1/ZO-2-dKO cells expressing ZO-1-GFP or a ZO-1-GFP mutant lacking PDZ2 domain (ZO-1 Δ PDZ2-GFP) with anti-ZO-1 mAb, anti-GFP pAb, or anti- α -tubulin mAb. **(D)** Double-immunofluorescence staining of ZO-1/ZO-2-dKO cells expressing ZO-1-GFP or ZO-1 Δ PDZ2-GFP with anti-GFP pAb and anti-angulin-1 pAb. Confocal sections in the apical region, including ZO-1 constructs and the lateral region, together with the corresponding Z-stack images along the white dotted lines are shown. Arrowheads indicate TCs. Bar: 10 μ m. **(E)** Pull-down assays of lysates of ZO-1/ZO-2-dKO cells expressing ZO-1-GFP or ZO-1 Δ PDZ2-GFP with GST-ang575. Bound proteins, input of lysates, and GST-ang575 used in the assay were analyzed by Western blotting with anti-GFP pAb and anti-GST pAb.

